



Spatial patterns in second-order impacts of human activity on climate, land and water

Hannah Zoller¹, Steven J. Lade^{1,2}, C. Kendra Gotangco Gonzales², Ingo Fetzer¹, Nitin Chaudhary^{1,3}, and Juan C. Rocha¹

¹Stockholm Resilience Centre, Stockholm University, Albanovägen 28, 10691 Stockholm, Sweden

²Fenner School of Environment & Society, Australian National University, Canberra ACT 2600, Australia

³Centre for Environmental and Climate Science, Lund University, Sölvegatan 37, 22362 Lund, Sweden

Correspondence: Hannah Zoller (hannah.zoller@su.se)

Abstract.

In order to assess the full systemic impact of anthropogenic pressures on climate and land, it is crucial to account for second-order impacts mediated by bio-geophysical processes, which typically display a high spatial heterogeneity. In this study, we systematically compare different clustering approaches to capture uni- and multivariate spatial patterns in second-order impacts of human activity on climate, land, and water. In a first step, we estimate effect sizes based on simulations from a spatial global vegetation model. In a second step, we approach the question of suitable spatial clustering. Following a top-down approach first, we map the global pattern of second-order impacts on common natural partitions of the Earth, like climate- or vegetation-zones. Cluster validity indices reveal a close alignment between the second-order impacts of land use change on climate and a biogeographic classification. In contrast, the second-order impacts of climate- and land use change on surface water runoff are best captured by the Köppen-Geiger climate zones. Following a bottom-up approach, we employ multivariate spatially constrained clustering to derive an integrative global partition. Several patches of tropical rainforest on the Indomalayan islands as well as large areas of warm grasslands in Australia are identified as high-impact clusters. The results of this study should be considered illustrative as they are based on only one dynamical vegetation model. Nevertheless, they emphasize the local nature of second-order impacts and elucidate both the potential and risks of spatial aggregation.

15

1 Introduction

Anthropogenic pressures on critical Earth system processes are continuously increasing and have driven the Earth beyond its safe operating space (Richardson et al. (2023)). This underscores the necessity for a more profound understanding and governance of these pressures (Gupta et al. (2024)). However, understanding the impact of a human disturbance often goes beyond assessing solely its direct effect - it further requires accounting for the biophysical interplay between different Earth

20



system processes, leading to second-order impacts. Exemplarily, while the *direct* impact of deforestation is a decrease in natural vegetation, potential *second-order* impacts include an increase in surface water runoff or a decrease in carbon storage.

On a global level, taking account of second-order impacts can amplify the measured impact of disturbances in many cases (Lade et al. (2020)). At the local level, the situation is much more complex, as a multitude of studies on the interplay between climate change, vegetation cover, and the water cycle demonstrate (Piao et al. (2007), Jong et al. (2013), Sterling et al. (2013), Ito and Inatomi (2012), Zhou et al. (2023)). The magnitude of these effects can vary strongly across regions and corresponding studies typically report them in a spatially aggregated format. For instance, Cramer et al. (2001) and Tobian et al. (2024) assess the effects of climate change for different vegetation zones. Luo et al. (2008) consider these effects depending on the climate zone, while Betts et al. (2007) aggregate them by continent. Koirala et al. (2017) quantify groundwater-vegetation interplay by climate zone in combination with forest type, Lade et al. (2021b) average interaction strengths by continent and dominant functional vegetation type. However, any type of aggregation comes at the cost of information loss, and it remains unclear if these aggregation approaches are indeed fit for purpose. In particular, a classification by functional vegetation type generally does not represent patterns of terrestrial carbon, water, and energy flux regimes; it might even obscure the real world behavior of ecosystems (Page et al. (2023)). Instead, other ecosystem characteristics, such as soil attributes, topography, or site hydrology and disturbance, might be essential to capture these functional regimes (Page et al. (2023)). So why aggregate at all? Beyond a reduction in computational costs, usability and communicability of results play a crucial role. Especially in studies at the interface between science and policy, coherent clusters rather than a highly resolved pattern can increase accessibility and encourage the use of scientific findings in decision-making.

In this study, we systematically compare the ability of different Earth partitions to capture the spatial heterogeneity of second-order impacts of human pressures on climate and land. We derive potential environmental drivers of these effects, and demonstrate the risk of information loss that comes with established aggregation approaches. First, we assess the magnitude of second-order impacts on crucial climate, land, and water processes. Our estimations rely on simulation output of the one-way coupled, spatially resolved dynamical vegetation model Lund Potsdam Jena managed Land (LPJmL, Schaphoff et al. (2018)). Finally, this study addresses the question of appropriate aggregations. Following a top-down approach first, we test the ability of established partitions of the Earth to capture the uni- and multivariate spatial pattern of second-order impacts. Our analysis covers a wide range of classification criteria, ranging from geographical, to climatic and biotic criteria, yielding indications of potential drivers of the different effects. Following a bottom-up approach, we derive spatial clusters of second-order impacts using a multivariate clustering based on soft spatial constraints (Chavent et al. (2018)). The resulting integrative Earth partition sheds light on the local interplay of second-order impacts, acknowledging the fact that from a systemic view, such an integration is substantial for a holistic assessment of anthropogenic pressures (Lade et al. (2021b)).



2 Data and methods

We quantify second-order impacts on climate, land, and water in a high spatial resolution (Section 2.1). The resulting global maps form the basis for a top-down clustering (Section 2.2) and bottom-up clustering approach (Section 2.3). The quality of a clustering is assessed via clustering validity indices (Section 2.4). Figure 1 illustrates the structure of this study.

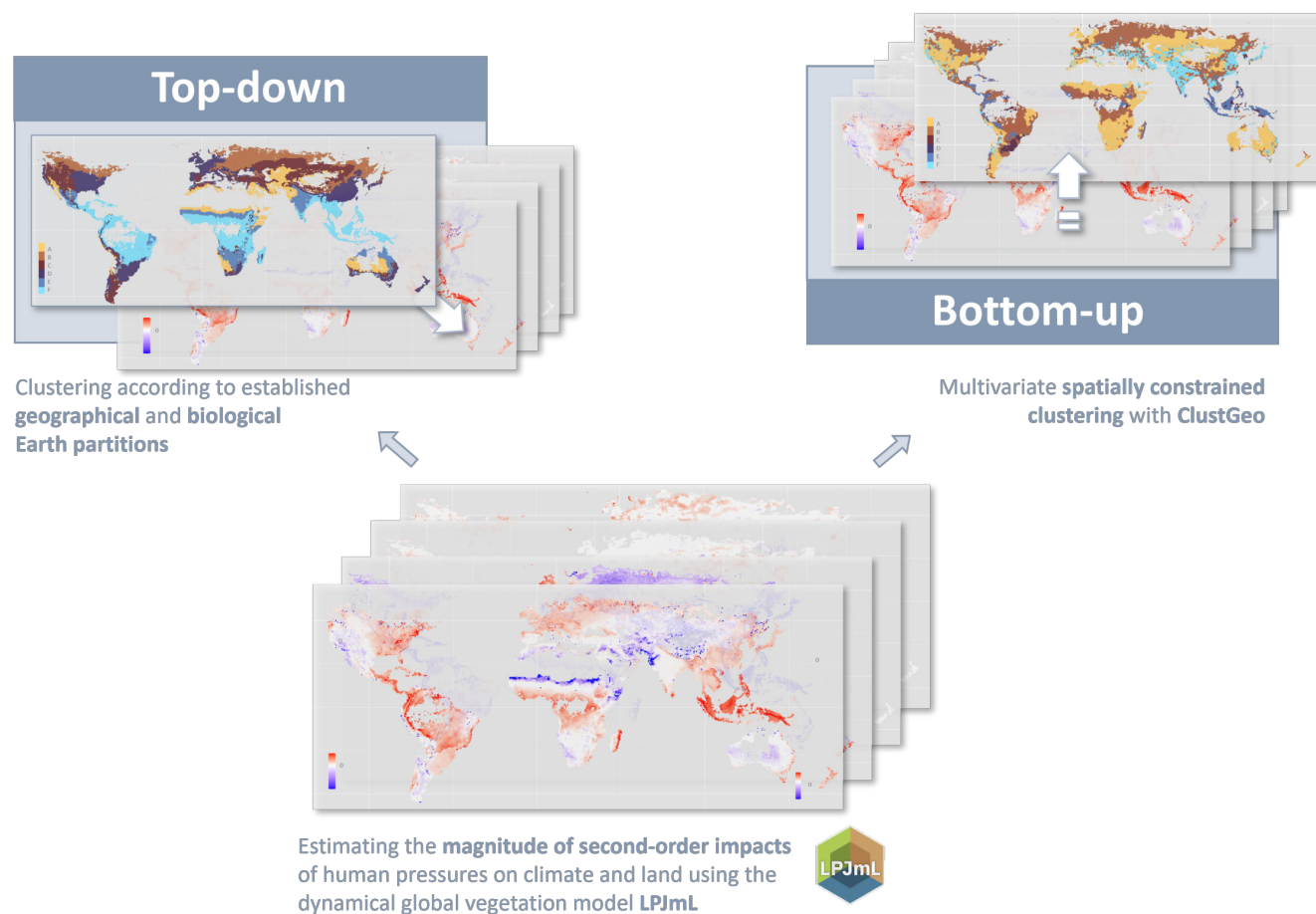


Figure 1. Conceptual workflow. In a first step, we estimate the magnitude of second-order impacts of human pressures on climate and land leveraging the dynamical global vegetation model LPJmL. Based on the resulting maps, we compare the ability of established Earth partitions to capture the resulting spatial patterns (top-down approach), and we derive optimal partitions applying the clustering algorithm ClustGeo (top-down approach).

55 2.1 Estimating the strength of second-order impacts

We estimate the magnitude of the effects of change in atmospheric CO₂ concentration on surface water runoff and natural vegetation cover, as well as the magnitude of the effects of land use change on surface water runoff and carbon storage density



(Fig. 2). The estimates rely on LPJmL simulation outcomes at a 0.5° spatial resolution for the years 1901 to 2013, as being provided by Lade et al. (2021b). Simulations are driven by the re-analysis dataset CRU TS3.21, a monthly climate dataset over all land domains except Antarctica, derived from an extensive network of weather observation stations (Harris et al. (2014)). The one-way coupling of the model allows isolating particular effects without the need to disentangle overlapping feedback effects. Runs are repeated with and without human land use, represented by the conversion of natural vegetation to cropland (Schaphoff et al. (2018)).

We extract the following variables per year and per 0.5° by 0.5° tile from each run: the percentage of the tile covered by natural vegetation as a proxy of the land component, the surface water runoff density (mm yr⁻¹) as a proxy of the water component, and the carbon storage density (g m⁻²) as one of the proxies of the climate component.

While largely following the estimation procedure by Lade et al. (2021b), our quantification of land use slightly differs. It rather aligns with the measure of biosphere integrity used by the Earth Commission, which measures the amount of natural ecosystems below which some ecosystem services are lost (Mohamed et al. (2024)).

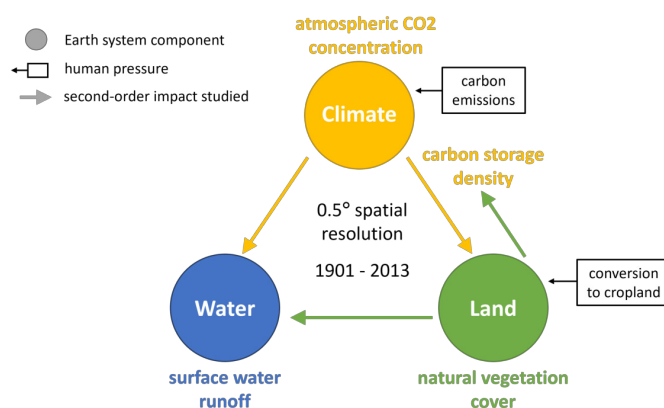


Figure 2. Modeling set-up. We use LPJmL simulation outcomes for the years 1901-2013 in a 0.5° spatial resolution to estimate the strength of second-order impacts that human pressures in the form of carbon emissions and in the form of conversion of natural vegetation to cropland have on carbon storage density (climate), natural vegetation cover (land), and surface water runoff (water).

The effects of change in natural vegetation cover are quantified using simple difference quotients. More precisely, its effect on runoff is measured via the difference in average runoff (RO) during the last 30 years of simulations with (wLUC) and without human-driven land use change (noLUC) in a tile, divided by the difference in average vegetation cover (VC) during the last 30 years of simulations with and without human-driven land use change in the same tile, i.e.

$$VC \rightarrow RO = \frac{RO_{wLUC} - RO_{noLUC}}{VC_{wLUC} - VC_{noLUC}} \quad (1)$$

The effect of change in natural vegetation cover on climate, measured via carbon storage density (C), is defined analogously. Observe that, consequently, if the average vegetation cover in a grid cell is the same in the last 30 years of the scenario with and the scenario without land use change, the size of the effect cannot be computed. Acknowledging the fact that the raster



approach is more prone to noise than the aggregated approach, we exclude grid cells whose difference in vegetation cover is less than 1 % of the total area, assuming that such marginal changes do not reflect change in human land use but noise in the simulation and can therefore be neglected.

The effects of climate change on runoff and vegetation cover are evaluated on the basis of the scenario without human-driven change in land use. In contrast to the first approach, we make use of the total length of the simulation by regressing yearly runoff density/natural vegetation cover per tile on global CO₂ concentrations between 1901 and 2013 and, whenever significant ($p \leq 0.05$), considering the regression coefficient as magnitude of the respective effect. Note that this magnitude might reflect both *direct* effects of climate on water, such as through changes in precipitation, and *indirect* effects mediated through changes in natural vegetation cover, such as variations in the soil infiltration rate.

To diminish the effect of outliers in clustering and cluster validation, we “clip” each of the four data sets to effect-dependent upper and lower boundaries. More precisely, we increase or decrease, respectively, all values below or above certain boundaries [c_{\min}, c_{\max}] to the respective boundary. The boundaries were set to $[-50, 25]$ (VC → RO), $[-2000, 4000]$ (VC → C), $[-2, 1.5]$ (C → RO), and $[-0.005, 0.005]$ (C → VC).

We repeat the whole estimation procedure relying on LPJmL simulations driven by six different climate models (CanESM2, GFDL-CM3, GFDL-ESM2G, HadGEM2-AO, MIROC-ESM, NorESM1-ME), provided by Lade et al. (2021a).

2.2 The top-down approach: Natural partitions of the Earth

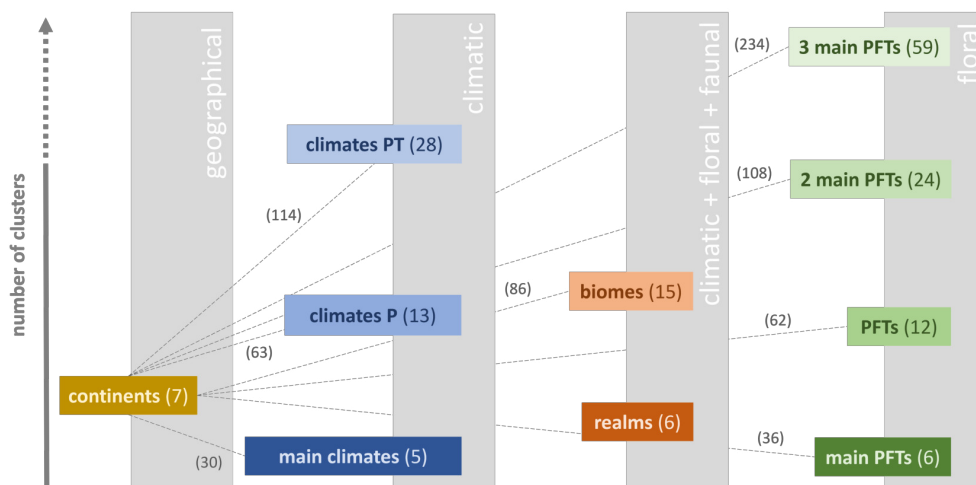


Figure 3. Creating combined Earth partitions. Base partitions are ordered along the x-axis according to the nature of their classification criteria and along the y-axis according to their number of clusters. As exemplarily depicted for continents, we furthermore create combined partitions. The numbers in brackets indicate the number of clusters. (Nomenclature: climates P = main climates + precipitation conditions, climates PT = main climates + precipitation conditions + temperature conditions (compare Table B1), PFTs = plant functional types as defined by LPJmL, classification by the (one/two/three) most dominant PFTs in a tile.)



We cluster the spatially resolved second-order impact sizes according to ten base partitions and certain combinations of these
95 partitions (Figure 3). Continents (N=7) provide an apparent geographical partition (Lade et al. (2021b)). The Köppen-Geiger
climate classification offers a simple climate partition (Kottek et al. (2006)), starting from five main climates, but refined by
taking into account precipitation (N=13) and temperature profiles (N=28) (Kottek et al. (2017)).

Our vegetational Earth partitions are based on the continuous distribution of the dominant plant functional types (PFTs) as
defined by the LPJmL global dynamic vegetation model outputs (N=12) (Schaphoff et al. (2018)). The classification is based
100 on the average fractional cover over the last 30 years of the simulation without human-driven land use. With this choice, we
follow both Lade et al. (2021b) and Dinerstein et al. (1995) in their approach to base their classifications on the original land
cover before intense human-induced changes. Aggregating plant functional types into five main types (N=6, including barren
land) following major regional attributes yields a coarser partition, while characterizing tiles by their two (N=24) and three
(N=59) most dominant PFTs results in finer partitions.

105 Biogeographic realms (N=6) have been defined as continent- or sub-continent-sized areas with unifying geographical, floral,
and faunal features (Udvardy (1975); Dinerstein et al. (2017)). Each realm can be further divided into different biomes (N=15),
characterized by a comparable climatic regime, similar vegetation structure and spatial patterns of biodiversity (Dinerstein
et al. (1995); Ostberg et al. (2013)). Biome classification is based on the averaged results of the last 30 years of the LPJmL
simulation without human-driven land use.

110 We furthermore consider combinations, “overlaps”, of two partitions each, by classifying tiles according to their respective
classes in both partitions. Simply put, if partition A distinguishes between classes A_1 and A_2 , and partition B between classes
 B_1 and B_2 , the combined partition AB consists of classes A_1B_1 , A_1B_2 , A_2B_1 , and A_2B_2 . We combine each of the rough
partitions (continents, main climate types, realms, and main PFTs) with all other partitions except for their own refinements.
Figure 3 illustrates the combination scheme using the example of continents. Note that we do not consider the overlap of
115 continents and realms due to their high similarity. Maps of all base partitions can be found in Appendix A.

2.3 The bottom-up approach: Spatially constrained clustering

In preparation for the multivariate clustering, we reduce the data space to tiles in which the natural vegetation cover does
differ between the simulation with human-driven land use change and the one without (35.800 out of 67.420 tiles). This pre-
processing step makes sure that all four effect-types can be estimated on each tile considered and thereby reduces a potential
120 bias towards certain effect types in the cluster validity indices. Furthermore, to reduce biases in the clustering results, we
rescaled the data set for each effect to $[-1, +1]$ by dividing each value by the maximal absolute value of the respective effect
size.

The R-package ClustGeo provides a hierarchical clustering algorithm with spatial constraints, taking into account both the
similarities in the “feature space” (in our case the four effect variables) and the similarities in the “constraint space”, defined by
125 spatial attributes of the data points (Chavent et al. (2018)). For our analyses, we use Euclidean distances between multivariate
effect sizes to measure similarity in the feature space.



We implement similarity in the constraint space in two different ways. At first, in form of a simple binary matrix, where a “1” denotes that two grid cells are horizontally, vertically, or diagonally neighboring. This definition of similarity leads, loosely speaking, to topologically “smooth” clusters. Nevertheless, since ClustGeo is based on *soft* spatial constraints only, clusters can consist of several unconnected, geographically dispersed components. This mimics the shape of the clusters in many of the top-down partitions considered in this study. Therefore, the neighborhood-based similarity measure is well-suited for comparing the performance of top-down and bottom-up partitions.

For an aggregation into geographically more interpretable clusters, we repeat the clustering procedure defining dissimilarity in the constraint space as geographic distance between the tiles’ centroids. Intuitively, basing the definition of dissimilarity on distance rather than neighborhood typically results in less smooth, but spatially more compact clusters.

The so-called mixing parameter $0 \leq \alpha \leq 1$ allows us to balance geographic cohesion and homogeneity within the group in the resulting partition. Increasing α from 0 will result in topologically/spatially more compact clusters, potentially at the cost of similarity of effect size within clusters.

We repeat the clustering procedure for various combinations of the number of clusters K and the mixing parameter α . We range K from 5 to 255 in steps of 10 and α from 0.1 to 0.7 in steps of 0.2.

2.4 Measuring clustering performance

We assess the quality of both natural Earth partitions and bottom-up clusterings via established cluster validity indices. Typically, the quality of a partition is characterized by two aspects: the similarity of the elements within a cluster (“compactness” or “homogeneity”), and the distance between clusters in the feature space (“separation”) (Todeschini et al. (2024)).

Assume that n objects are being clustered in K disjoint clusters. Let d be the number of variables (i.e., the dimension of the feature space) and \mathbf{x} the d -dimensional feature vector of object x . Here, \mathbf{m} denotes the d -dimensional vector of variable means, \mathbf{m}_k the d -dimensional vector of cluster means. We denote by n_k the number of objects of the cluster k . We use the notation $\|\cdot\|$ for the Euclidean norm of a vector.

Independently of the underlying clustering, the total variability in the dataset is measured by the *Total sum of squares*

$$\text{TSS} = \sum_{j=1}^d \sum_{i=1}^n \|\mathbf{x}_i - \mathbf{m}\|^2.$$

It consists of the *Between-cluster sum of squares*

$$\text{BSS} = \sum_{k=1}^K n_k \cdot \|\mathbf{m}_k - \mathbf{m}\|^2,$$

quantifying the variability between clusters, and the *Within-cluster sum of squares* $\text{WSS} = \text{TSS} - \text{BSS}$. Typically, a large BSS or, equivalently, a small WSS are indicative of good cluster quality. Here, we consider an alternative to the WSS, the *Banfield-Raftery index*



$$BR = \sum_{k=1}^K n_k \cdot \log \left(\sum_{i=1}^{n_k} \|\mathbf{x}_i - \mathbf{m}_k\|^2 / n_k \right),$$

155 which is better adapted to large differences in cluster size (Todeschini et al. (2024)). For a slightly different angle of perspective (although, of course, not independent), we further consider the *R-squared* index

$$RS = \frac{BSS}{TSS},$$

which quantifies the fraction of total variability in the data set that is explained by the differences between clusters. Consequently, a value close to 1 is typically more desirable than a value close to 0.

3 Results and Discussion

160 Compared to the extensive patterns of second-order impacts of land use change (Figs. 4A-B), the second-order impacts of climate change on water runoff and natural vegetation cover exhibit more “patchy” patterns without a clear dominance in sign (Figs. 4C-D). This phenomenon reflects the complex interplay of land-atmosphere interactions in response to increasing levels of atmospheric carbon concentration (Zhou et al. (2023)). Furthermore, in many regions, we observe only weak or no significant second-order impacts of climate change. While this phenomenon may be partly due to opposite effects canceling each other out, it is also likely to be exacerbated by differences in the methods used to estimate effect sizes (see *Methods*).
165 We provide a detailed discussion of the spatially resolved maps of effect sizes and a comparison to corresponding studies in Appendix C.

3.1 Comparing the clustering quality of top-down and bottom-up partitions

With respect to explained variability, the selected top-down partitions are in general clearly outperformed by the bottom-up partitions. The R-squared index of the neighborhood-based bottom-up partitions without spatial constraints ($\alpha = 0$) converges
170 towards a value of 1 for all four effect types (Fig. 5). With increasing spatial constraints ($\alpha = 0.1, 0.3, 0.5, 0.7$), within-cluster variability naturally increases, leading to a lower between-cluster variability and thereby to a decrease in the R-squared index. Nevertheless, in most cases there remains a large gap in explained variability between the bottom-up and the top-down partitions, which do not exceed values of 0.3 for the effects of climate change (Fig. 5C+D) and values of 0.5 for the effect of land use change on water runoff (Fig. 5A). Only for the effect of land use change on climate, RS indices exceed values of 0.7,
175 indicating that more than 70 % of the total variance in size of second-order impacts is explained by the variance among cluster means (Fig. 5B). The high performance in this particular case might be traced back to the fact that measuring the effect of land use change on vegetation carbon density provides a very direct and unconfounded approximation. As such, its strength reflects the vegetational and climatic characteristics of an area - each of which are captured by several top-down partitions and, in a combined fashion, by the biome framework.

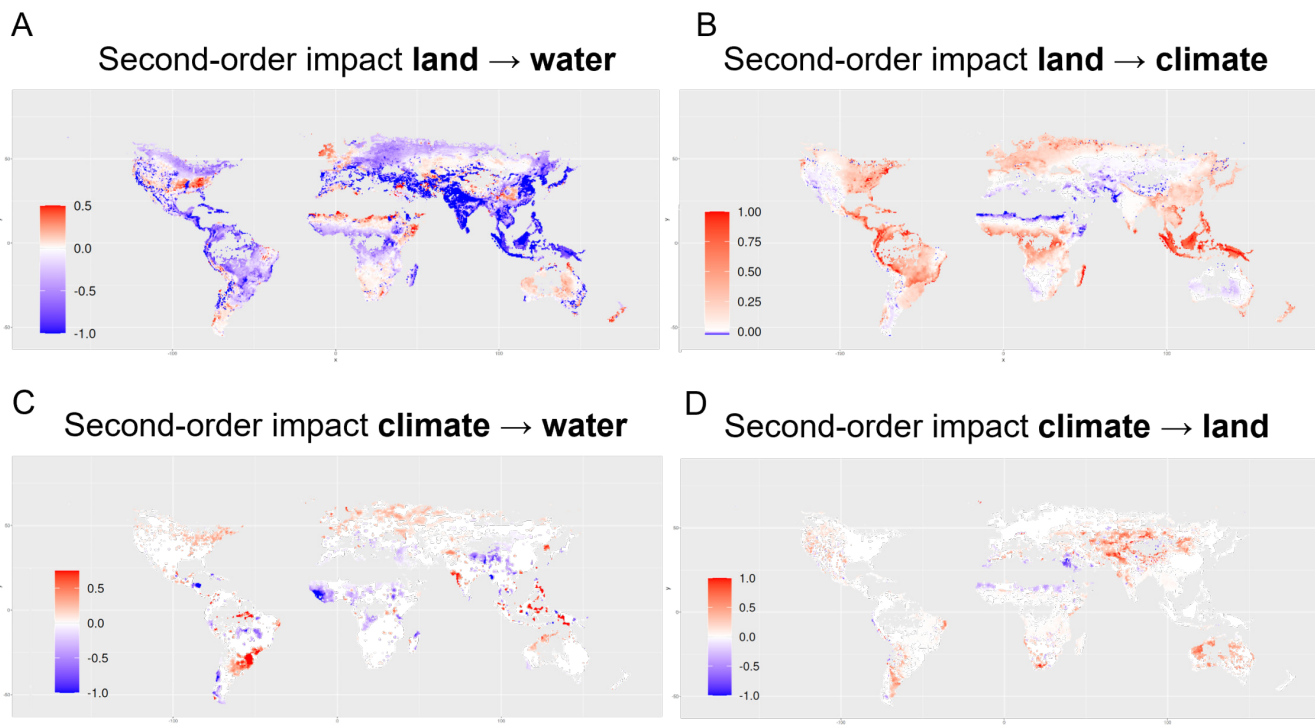


Figure 4. Global patterns of second-order impacts. The maps show the scaled effect sizes of changes in natural vegetation cover on (A) surface water runoff and on (B) carbon storage and of changes in atmospheric carbon dioxide concentration on (C) surface water runoff and on (D) natural vegetation cover. A positive effect size (red) indicates that an increase in one Earth system process (e.g., increased natural vegetation cover) causes an increase in another Earth system process (e.g., increased surface water runoff). Analogously, negative effect size (blue) indicates that an increase in one process leads to a decrease in another. Note that for clarity, the color scale varies across effect types and directions and therefore should not be used for cross-comparisons. All maps are restricted to grid cells in which the cover of natural vegetation has changed by more than 1 % of the cell area between the simulations with and without human-driven land use change (see *Methods*). World maps showing the larger area of estimated effects of climate change on surface water runoff and natural vegetation cover can be found in Fig. G1.

180 If performance is being assessed via within-cluster variability (BR index), the difference between the two approaches is not as clear. Intuitively, the BR index overall increases with increasing spatial constraints (Fig. F1). Interestingly, for the effects of climate change (Fig. F1C+D), top-down partitions show a smaller within-cluster variability than equally-sized bottom-up partitions under strong spatial constraints ($\alpha = 0.5$ and $\alpha = 0.7$). For the effect of land use change on climate, some of the top-down partitions perform even better than the corresponding unconstrained bottom-up partitions (Fig. F1B). There are

185 several reasons why the unconstrained clustering algorithm might not always produce a clustering that optimizes the BR index. Firstly, the algorithm minimizes with respect to a slightly different measure of within-cluster variance. Secondly, the algorithm optimizes at each step, meaning it can end up in local rather than global optima (compare Chavent et al. (2018)).

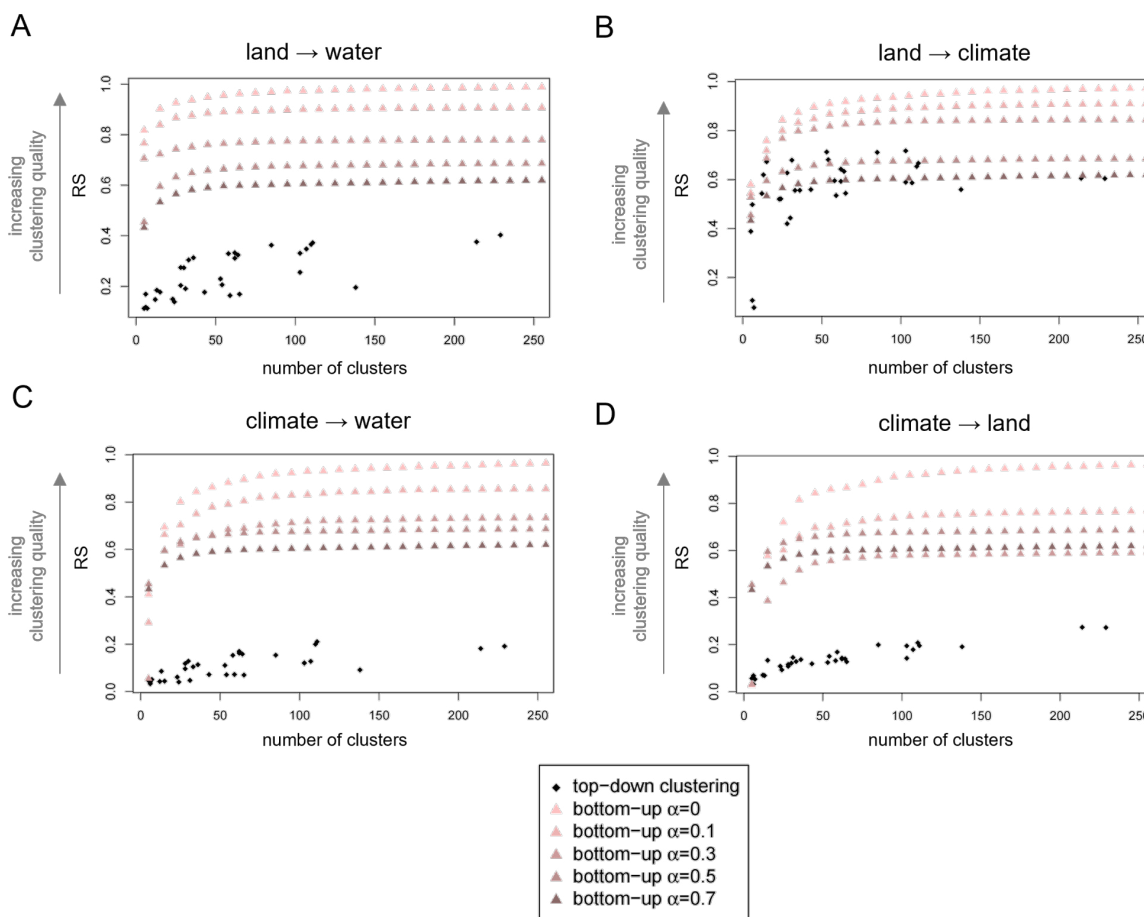


Figure 5. Bottom-up clustering substantially outperforms top-down clustering. R-squared index (RS) of the “top-down” geographical, climatic and biological Earth partitions and of the “bottom-up” neighborhood-based partitions without ($\alpha = 0$), and with increasing spatial constraints $\alpha = 0.1, 0.3, 0.5$, and 0.7 . As these partitions topologically resemble the top-down partitions, we consider their RS and BR (Banfield-Raftery) indices as “baselines” for the clustering potential of the dataset. Performance is evaluated separately based on the one-dimensional feature space of effect size for (A) the effect of land on water, (B) land on climate, (C) climate on water, and (D) climate on land, respectively. The partitions are sorted by their number of clusters. Intuitively, the RS index increases with increasing number of clusters k and the algorithm yields the best results without spatial constraints ($\alpha = 0$).

3.2 The top-down approach

3.2.1 Identifying drivers of second-order impacts

190 We find that the spatial patterns of individual second-order impacts are best explained by different classification criteria (Figure 6). The effects of land use change and of climate change on surface water runoff are best represented by climate-based partitions



(Fig 6A+C). The BR indices align with this trend (see D1). With an RS index of 0.21, the classification by continent and Köppen-Geiger climate zone (climates PT) provides the best match for the global pattern of the climate → water effect. The same partition is among the best matches for the pattern of the land → water effect with an RS value of 0.37.

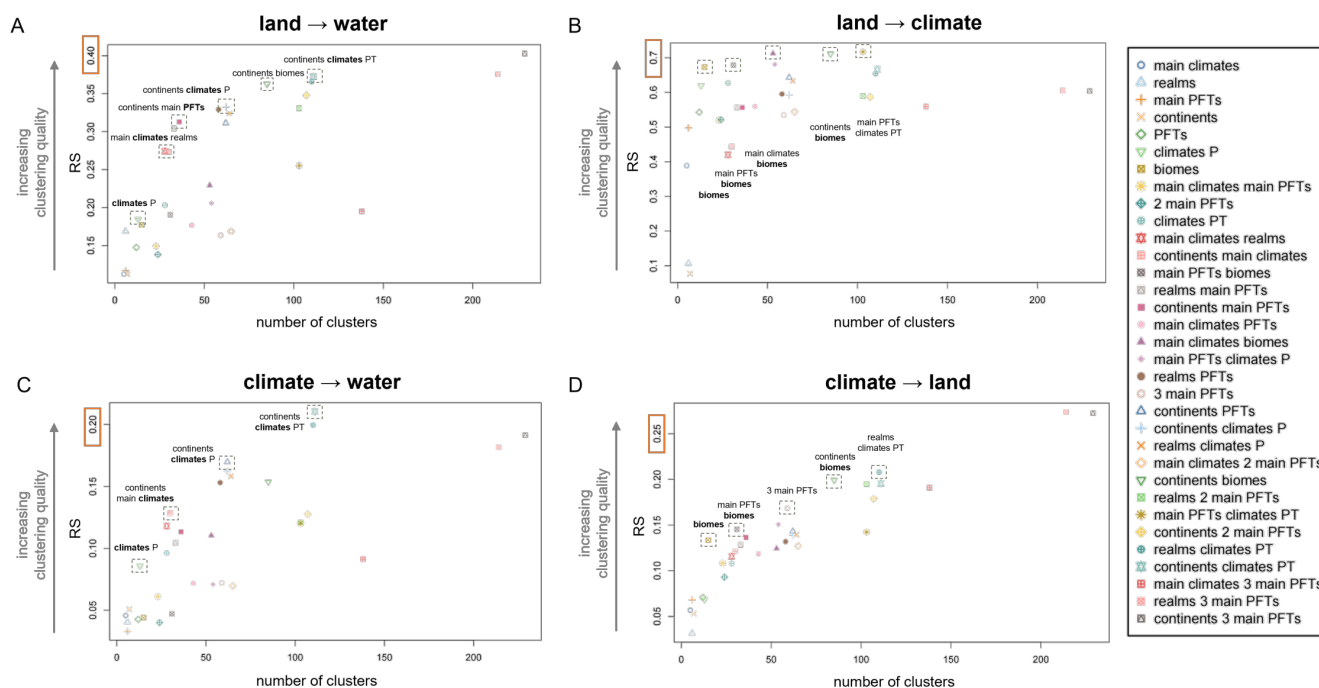


Figure 6. Spatial patterns of individual second-order impacts are best explained by different natural classification criteria. R-squared index (RS) of the 33 geographical, climatic, and biological Earth partitions with respect to the magnitude of the effects of land use change on (A) surface water runoff and (B) carbon storage, as well as the magnitude of the effects of change in carbon dioxide concentration on (C) surface water runoff and (D) natural vegetation cover. The partitions are sorted by their number of clusters k and highlighted by a square if they stand out in performance compared to partitions of similar number of clusters.

195 The best-performing partitions suggest potential environmental drivers of individual second-order impacts. We find that changes in natural vegetation cover have a particularly strong negative effect on surface water runoff in the Indomalayan realm. This includes clusters such as the Asian rainforest (Af) and the Asian Steppe (BSh) (Fig. H1A). Furthermore, four of the five clusters exhibiting the strongest negative impact are rainforests (Af). A strong positive effect size can be observed in the hot desert (BWh) of Africa. One cluster for which it is particularly apparent that the pattern of effect size is not well represented by an average value is the fully humid, hot summer region (Cfa) in eastern North America, indicating driving mechanisms beyond
 200 an average value is the fully humid, hot summer region (Cfa) in eastern North America, indicating driving mechanisms beyond climate and precipitation. Here, the distinctive nature of the Mississippi River ecosystem is not reflected by the Köppen Geiger climatic boundaries.

The effect of climate change on the availability of surface water runoff (Fig. H2A) is strongly positive in the fully humid, hot summer region of South America (Cfa). In contrast, the Asian tundra (ET) is characterized by a notable negative effect size,



205 i.e. an increase in climate change causes a strong decrease in surface water runoff. The overall similar means and high standard deviations across the clusters align with the generally weak performance of the cluster validity indices and demonstrate the apparent mismatch between the “patchy” pattern of effect size and the more extensive pattern of clusters in the natural partition (Fig. H2B).

Across the four effect types, the top-down partitions yield the highest RS values and the smallest BR values for the effect of land use change on climate (Fig. 6B, D1B). Here, it is not the purely climate-based but the biome-based partitions that stand out in performance. The classification by continent and biome yields an RS value of 0.71, indicating that the differences between the means of the underlying 85 clusters explain more than 70 % of the total variability in the dataset. Taking a closer look at the clustering by continent and biome, we observe an extensive high positive effect size in the Asian Tropical Rainforest (Fig. H3), aligning with the high carbon storage capacity of this vegetation type Lade et al. (2021b). The reverse effect occurs in the African Desert, where a conversion to cropland apparently increases the carbon storage capacity of an area. This effect might be due to the natural vegetation occurring on cropland between growing seasons. The boundaries of the North American Temperate Broad-leaved Deciduous Forest remarkably well separate areas of higher to moderate effect size from areas of little to no effect further westward. The border between the South American Rainforest and the Temperate Broad-leaved Deciduous Forest provides another example of an exact separation between regions of different levels of effect size. The generally well-separated means of effect size across the clusters visually support the high clustering quality indicated by the cluster validity indices (Fig. H3B).

For the effect of climate change on natural vegetation cover, we observe a similar trend towards biome-based partitions as for the reverse effect of land use change on climate (Fig. 6D, D1D). Since those partitions combine climatic and vegetational characteristics, we consider this outcome to be a proof of concept rather than a new insight. In contrast to the high correspondence between the top-down partitions and the land → climate effect pattern, RS indices do not exceed values of 0.3 in the case of the climate → land effect. Consequently, just like for the effect of climate change on water, cluster means are generally not well separated across clusters (Fig. H3B). As mentioned earlier, the high interplay of different, partly opposing land-atmosphere interactions is likely to result in a complexity which the rather simple top-down partitions considered in this study might not be able to capture. A combination of more than two classification factors and/or the inclusion of further criteria (e.g., topographic factors) might yield further insights.

3.2.2 Revealing the risk of information loss

Assessing clustering quality in the multidimensional feature space of all four effect types confirms the earlier observed quality gap: while RS values exceed 0.9 for bottom-up partitions without spatial constraints and values of 0.5 for $\alpha = 0.7$, they do not exceed values of 0.4 for top-down partitions (Fig. F2A). A similar, albeit smaller discrepancy in performance can be seen for within-cluster variability (Fig. F2B). For partitions of fewer than 100 clusters, the multivariate pattern of effect sizes is best represented by a classification by continent and biome in terms of both explained variability and within-cluster homogeneity (Fig. E1). Only marginally higher RS indices and lower BR indices are yielded by larger partitions.

The best-performing partition of fewer than 50 clusters is provided by the classification by continent and main plant functional



types, as used in Lade et al. (Lade et al. (2021b)). However, this aggregation entails a significant loss of information. For the
240 comparison, it should be noted that Lade et al. normalize their *interaction strengths* with respect to the pre-industrial values
of the variables and the estimated guardrails for safe levels of impact. Consequently, they consider increases and decreases in
pressure on the respective Earth system processes, which leads to the opposite sign for their interaction value compared to our
climate change effect size. For example, consider the effect of land use change on surface water runoff in the temperate forest
region in North America. Lade et al. observe a slight negative interaction strength in this cluster (Fig. 3 in Lade et al. (2021b)).
245 When averaged across the corresponding tiles, our results corroborate this trend (Fig. I1). However, the spatially resolved effect
size in Fig. 4A reveals that the cluster contains a distinctive area of strongly negative effect size along the Mississippi river,
which is surrounded by large areas of positive effect size. These opposing effects cancel each other out and, with the positive
effect of land use change on runoff being generally slightly lower than the strength of the negative effect, lead to a negative
average value. Note that this particular pattern is neither well represented by the climate-based division discussed earlier (Fig.
250 H1). Similarly, in the tropical forests of South America, distinctive areas of positive and areas of negative effects of climate
change on runoff (Fig. 4C) cancel each other out, resulting in a negligibly small average interaction strength for the cluster. As
a further example, consider the effect of climate change on water in the tropical forest of Africa (Fig. 4C). We find a negative
average effect size in the cluster, which aligns with the results of Lade et al.. However, our approach reveals a hotspot of
negative effect size in the Guinean forests, gradually decreasing northwards and eastwards along the forest-savanna ecotone.
255 This remarkable pattern is obscured by the aggregation approach by Lade et al.

3.3 The bottom-up approach

The RS index of the bottom-up partitions converges to values above 0.9 for all four values of α , indicating that more than
90% of the total variability in the data set is explained by the variability among cluster means (Fig. 7A). The increase in the
RS index for an increasing number of clusters is particularly strong for smaller partitions, while the curve clearly flattens with
260 partition size approaching 100. In contrast to the RS index, the Banfield-Raftery BR index displays a weaker convergence and
 α -dependent differences in quality remain comparatively large even for higher numbers of clusters (Fig. 7B). Considering the
univariate R-squared index RS, we find that the bottom-up partitions explain the variability in the effect of land use change
on surface water runoff better than the variability in the other effects (Fig. J1). Interestingly, with respect to within-cluster
similarity, as being measured by the BR index, the partitions perform best for the effect of climate change on natural vegetation
265 cover (Fig. J2).

When aiming for an interpretable, communicable, and high-quality partition of the Earth into impact zones, one needs to
find a compromise between a manageable number of clusters (as regulated by K), spatial locality of the clusters (as regulated
by α), and both high values of between-cluster variance and within-cluster similarity. While an optimal choice will always be
context-specific, we will explore the characteristics and the interpretative potential of impact zones by means of a representative
270 partition of the Earth into 65 impact zones.

With growing α , spatial coherency of the clusters increases (Fig. K1). For $\alpha = 0.1$, some clusters with a certain degree of
cohesion and spatial compactness can already be observed, such as in the boreal forests in northern Asia and in the tropical

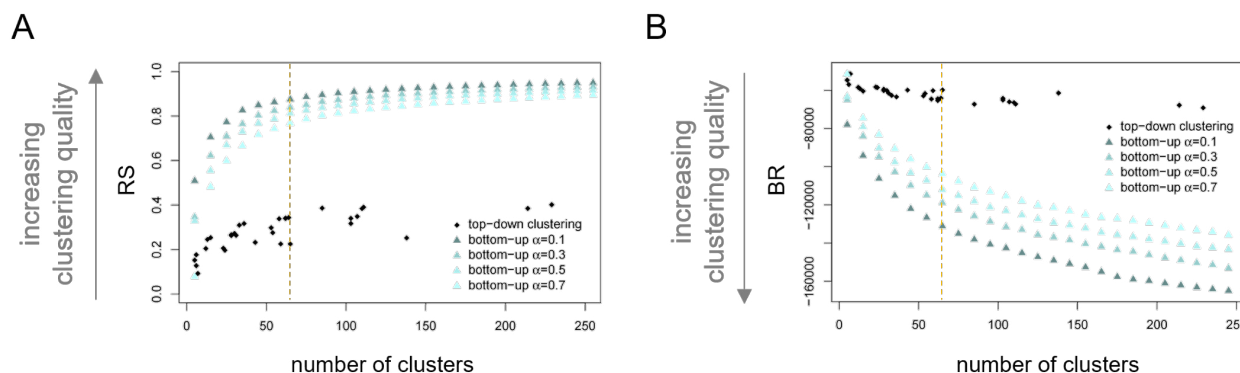


Figure 7. Performance of distance-based bottom-up partitions for varying mixing parameter α . (A) R-squared index (RS) and (B) Banfield-Raftery index (BR) for the distance-based bottom-up partitions generated by ClustGeo based on the multidimensional feature space of information strengths for the effects of natural vegetation change on surface water runoff and carbon dioxide storage as well as for the effects of change in carbon dioxide concentration on surface water runoff and natural vegetation cover. Indices are displayed for partitions generated with mixing parameter $\alpha = 0.1, 0.3, 0.5, 0.7$. With increasing α , i.e., an increasing amount of weight being assigned to the spatial constraints, clustering quality naturally decreases. This discrepancy is particularly pronounced for smaller numbers of clusters and decreases with increasing partition size. Partitions are ordered by their number of clusters. The dashed orange lines mark indices for the partition into 65 clusters, which we consider in more detail. For further orientation, we included the metrics of the top-down partitions presented in 3.2.

forests of Africa (Fig. K1A). Those impact zones reflect larger areas of uniform effect size in all four effect types, mirroring a natural spatial cohesion (compare Fig. 4). Overall, compared to the top-down partitions, the bottom-up partitions clearly reflect the more “patchy” pattern of effect size for the effects of climate change on water and natural vegetation (Fig. 4C-D). For $\alpha = 0.7$, the partition into 65 impact zones already explains 77 % of the total variability in the multivariate dataset (Fig. 7A) and the high level of spatial compactness allows for an interpretation of an observed impact profile in the context of a cluster’s regional environmental characteristics. In order to highlight patterns in the *interplay* of effects, our analysis will focus on clusters which stand out in absolute strength for at least two effect types (Fig. 8).

A frequent pattern in the clusters’ impact profile is the interplay of a negative effect of land use change on water and a positive effect of land use change on climate (Fig. K2). Hence, in the corresponding regions, the human-driven decrease in natural vegetation cover leads to an increase in surface water runoff and to a decrease in carbon storage density. These effects should be particularly strong in areas of dense vegetation with a high infiltration rate and carbon storage capacity, and indeed, the pattern is particularly strongly pronounced in the tropical forests of South America (Clusters 36 and 52), Africa (Cluster 48), and Asia (Clusters 35 and 54). While the estimated net effects of climate on land and water are generally low in the corresponding areas, there is one cluster which stands out by a markedly high effect size for the effect of climate change on surface water runoff: Cluster 44, which encompasses several patches on the Indomalayan islands. A closer inspection on Ecoregions level reveals that those patches largely overlap with montane rain forests and peat swamp forests. This observation suggests that the increase of the atmospheric CO₂ concentration leads to a comparably strong increase in surface water runoff in these types of



290 tropical and subtropical moist broadleaf forests. Piao et al. (2007) found a particularly strong increase in precipitation across large areas of the Indomalayan islands. Hence, we hypothesize that the remarkable effect on runoff could be resulting from a high sensitivity to increased rainfall due to the typically steep terrain and low infiltration rate of the soil in montane areas and due a potential saturation in peat swamp forests. We mark Cluster 44 as one of the “high impact” clusters, since second-order effect size is particularly strong for three different effects.

295 A less frequent pattern in the impact profile can be observed in warm savanna and open shrubland regions of Africa (Clusters 39 and 43), as well as in warm grassland regions of Australia (Cluster 60). Here, a human-driven decrease in natural vegetation cover leads to a decrease in surface water runoff and an increase in carbon storage density due to the apparently higher infiltration rate and storage capacity of cropland compared to sparse C4 grass. Note that Clusters 43 and 60 vary with respect to the effect of climate change on natural vegetation cover: while a change in atmospheric carbon dioxide concentration is largely
300 negatively correlated in the African cluster, it is strongly positively correlated with natural vegetation cover in the Australian cluster. We trace this observation back to the climate change-induced decrease in precipitation in the area of the former, and the increase in precipitation in the area of the later (Piao et al. (2007)). We classify the Australian cluster as high-impact cluster.

In several regions across North America (Cluster 21), Europe (Cluster 3), Asia (Cluster 18), and New Zealand (Cluster 65), we observe positive effects of human-driven land use change on both water runoff and carbon storage. In other words, in these
305 areas, a decrease in natural vegetation cover results in a simultaneous decrease in surface water runoff and in carbon storage capacity. Interestingly, the corresponding clusters all lie within areas that are dominantly covered by temperate forest, mixed with some C3 grass (compare Appendix A).

The effect size between land use change and runoff is strongly negative and the effect size between climate change and runoff strongly positive in Cluster 41, which encompasses several little patches in South America. While the former is typical for
310 rain forests, which dominate most of the patches, the latter could be the result of different effects. On the one hand, it could be traced back to a strong increase in precipitation in the corresponding areas (Piao et al. (2007)). On the other hand, a rising atmospheric CO₂ concentration typically leads to a decrease in transpiration and therefore an increase in soil moisture and runoff when vegetation cover is close to saturation (Zhou et al. (2023)).

Clusters 37, 47, and 38, all dominated by tropical forest mixed with temperate forests or C3 grass, are characterized by highly
315 negative effect sizes between climate change/land use change and surface water runoff. The later indicates that the CO₂-induced increases in vegetation cover exceed the effect of CO₂-induced decreases in transpiration (Zhou et al. (2023)). Cluster 38, encompassing Honduras and some larger patches on the Indomalayan Islands, additionally displays a highly positive effect size between land use change and carbon dioxide storage. We therefore classify this cluster as high-impact cluster.

A highly positive effect size between climate change and natural vegetation cover coincides with a negative effect size between
320 climate change and surface water runoff in the arid steppe of central Asia (Cluster 24). This impact profile is a clear indicator of the phenomenon just mentioned: climate-induced increases in vegetation cover exceed the effect of decreases in transpiration, leading to an overall decrease in surface water runoff. In Cluster 25, situated in the arid steppe of Asia as well, the positive effect size between climate change and natural vegetation cover coincides with a strongly negative effect size between human-driven land use change and surface water runoff.



325 3.4 Sensitivity analysis

The global pattern of second-order impacts is stable across climate models for the effects of land use change on surface water runoff and on carbon storage density (Figs. L1 and L2, respectively). Consequently, clustering analyses across all climate models support the observed dominance of climate-based aggregations for the effect on surface water runoff and the observed dominance of biome-based partitions for the effect on carbon storage density (Figs. M1 and M2, respectively). Note, however, that in the latter case, the dominant plant function type consistently appears as a crucial classification criterion as well (Fig. M2).

The variation across climate models is more noticeable for the effect of climate change on surface water runoff (Fig. L3). This might be due to the fact that the effect of climate change on runoff is composed of both direct and indirect effects mediated through changes in natural vegetation cover, further amplifying uncertainty. Nevertheless, four out of six climate models support our finding of a highly negative effect size in the tropical forest of Africa, with a hotspot in the Guinean forest. Based on the other two climate models, there is no significantly measurable effect in the corresponding cluster. Two out of four climate models support the highly positive effect size in the fully humid hot summer region in South America, based on the other four models there is no significant effect. While climate-based partitions are still strongly represented among the best-performing aggregations, the dominance across climate models is not as clear as for the historical re-analysis dataset (Fig. M3).

With respect to the effect of climate change on natural vegetation cover (L4), several of the observed patterns, such as the highly positive effect size in the temperate grassland of Asia and South America, are stable across climate models. However, there are two clusters which differ in sign of effect size. While the grasslands of central and eastern Africa are assigned a positive effect size based on three climate models, two of them imply a significant negative effect size. Only two of the climate models support the observed slight tendency towards biome-based partitions in the top-down clustering analysis (Fig. M4C+E), while the others either imply a high similarity of the spatial pattern to vegetation-based partitions or do not show a clear tendency.

3.5 Limitations of the study

The results presented in this manuscript build on simulations driven by historical re-analysis data. This approach naturally entails certain limitations. First of all, the reliability of re-analysis data like the one used in this study shows a strong spatial and temporal variation, reflecting the density of meteorological stations. Station coverage underlying CRU TS3.21 is generally high in large parts of North America (Fig. N1 A-D) as well as in central and western Europe (Fig. N1 C+D). Other areas, such as large parts of Brazil (Fig. N1 A+C) and northern Africa (Fig. N1 A+B), are particularly data-sparse in some variables, and respective values are heavily depending on interpolation (Harris et al. (2014)). Consequently, results affecting these areas should be interpreted with more caution. However, while this uncertainty might directly translate to the effect size of a single tile, we would like to point out that the main results presented in this manuscript are based on large-scale trends and therefore less sensitive to small deviations in the input data.



Models are always a simplified representation of reality. In this study, by choosing LPJmL as vegetation model, we opted for a *one-way* coupling. This implies, in particular, that our model does not directly capture feedback mechanisms, such as changes
360 in natural vegetation cover affecting the albedo of a region and thereby affecting climate. The inclusion of such processes could be subject of future studies. Furthermore, the estimation methods being used to quantify effect size (difference quotient and linear regression), capture only *linear* relationships (compare Lade et al. (2021b)). More complex causality detection methods (see e.g. Runge et al. (2019)) could yield a more refined picture and further enhance the current modeling set-up.

4 Conclusions

365 We systematically compared the ability of different spatial aggregation formats to capture the spatial pattern in second-order impacts of human pressures on climate and land. Following a top-down approach by clustering the Earth according to established natural classification criteria, we found that the spatial pattern of second-order impacts on surface water runoff is best explained by climatic classifications. In contrast, the spatial pattern of second-order impacts of land use change on carbon storage density is best explained by biotic classifications. While aggregation according to commonly known Earth partitions
370 facilitates communication, clustering quality appeared to be substantially higher when following a bottom-up approach. Based on the spatially constrained clustering algorithm ClustGeo, we derived an integrative partition based on the multivariate global pattern of second-order impacts on climate, land, and water. Among the resulting clusters, we identified several patches of tropical rainforest on the Indomalayan islands as well as large areas of warm grassland in Australia as high-impact clusters.

In order to generally move beyond simulation dependencies, a natural - although not trivial - next step would be the
375 extension of our framework to observational time series data. Going beyond the controlled set-up of simulations entails additional challenges such as the identification and the disentanglement of scale- and time-dependency, lagged effects, shared environmental drivers, and general higher-order effects. Eventually, a comparison of simulation- and observation-based world maps of second-order effects of human activity would also provide insights into the usability of LPJmL in future systemic assessments of anthropogenic impact on the Earth.

380 *Code and data availability.* Our results are based on the LPJmL simulation data by Lade et al. (2021a). The computation of the global station coverage uses the CRU TS3.21 dataset by Harris (2013). The R code underlying our results is provided as supplementary material to this manuscript.

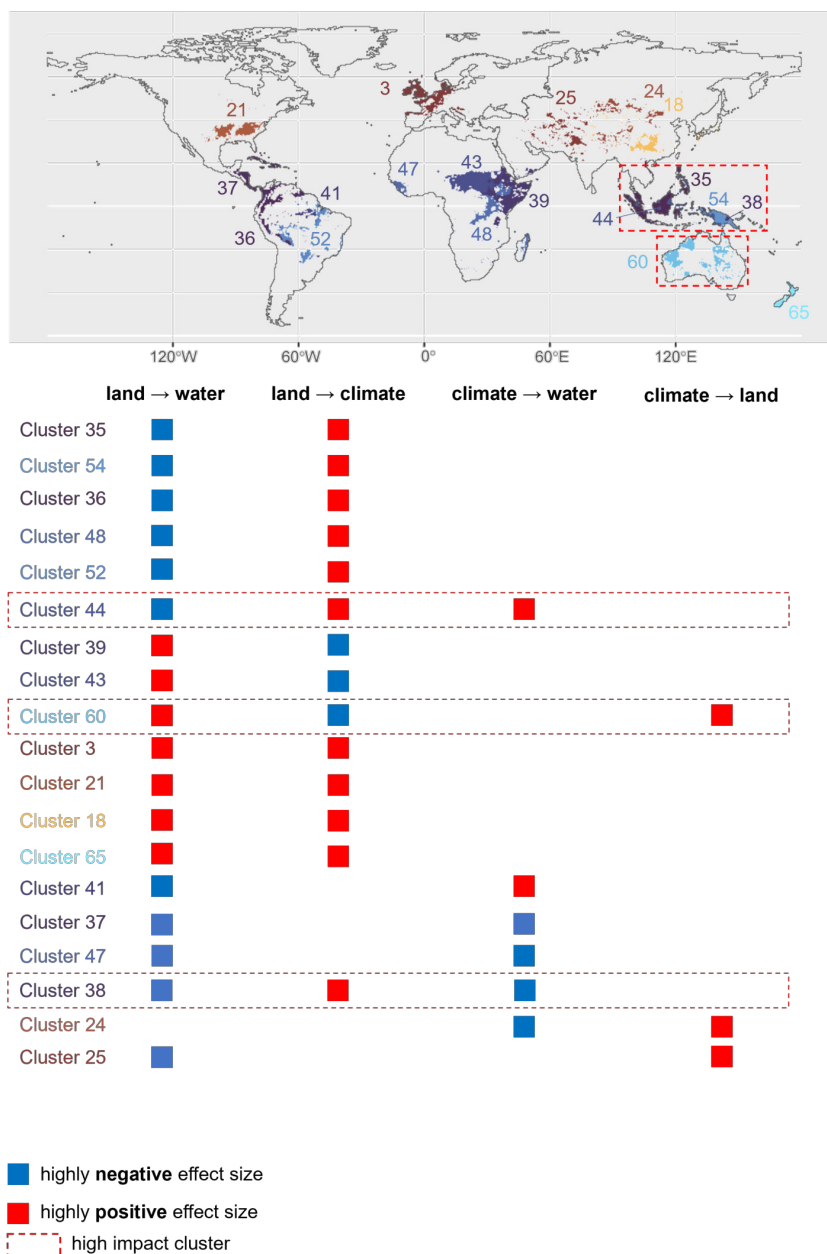


Figure 8. Integrative world map of bottom-up impact zones. The borders mark selected out of the 65 clusters that were generated by applying ClustGeo to the four-dimensional feature space of size of the effects of land use change on water and climate, as well as the effects of climate change on water and land use. The constraint space was given by geographical distances, and the mixing parameter α was set to 0.7. The table lists the impact profile of clusters which stand out in effect size for at least two different effect types. Red tiles indicate highly positive effect size, blue tiles highly negative effect size. Clusters with markedly strong (absolute) size of at least three effects are further emphasized as “high impact” clusters. Color and number code of the clusters aligns with that of the mean and standard deviations in Fig. K2.



Appendix A: Natural Earth partitions

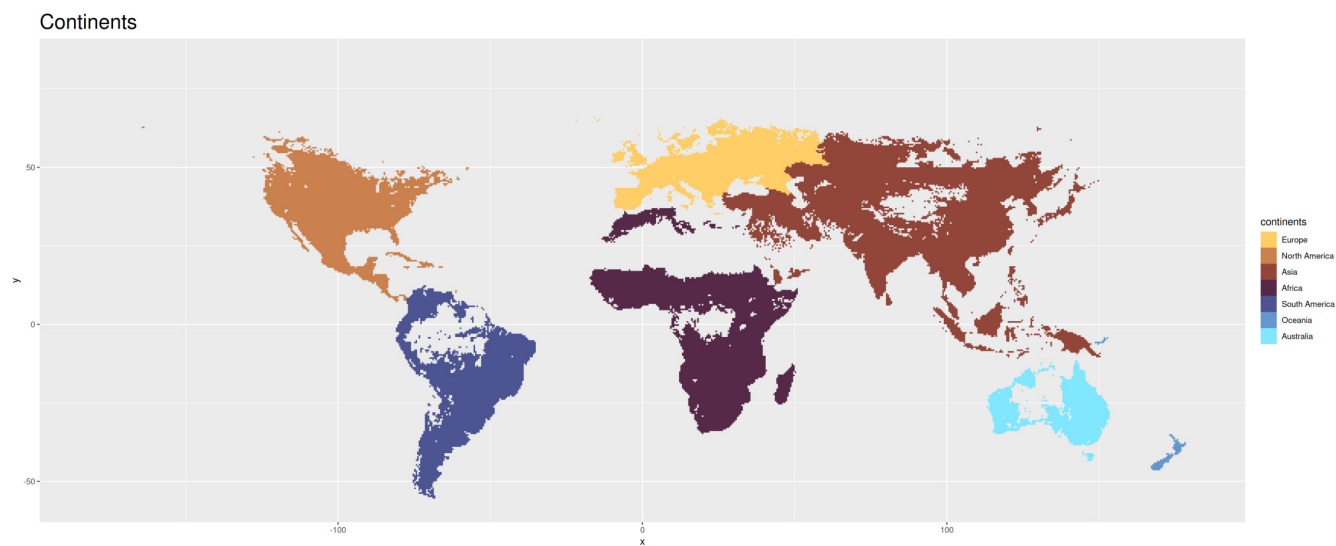


Figure A1. Geographic partition of the Earth into continents. Note that all maps in Appendix A display only tiles for which the size of all four effects could be computed (compare *Methods*).

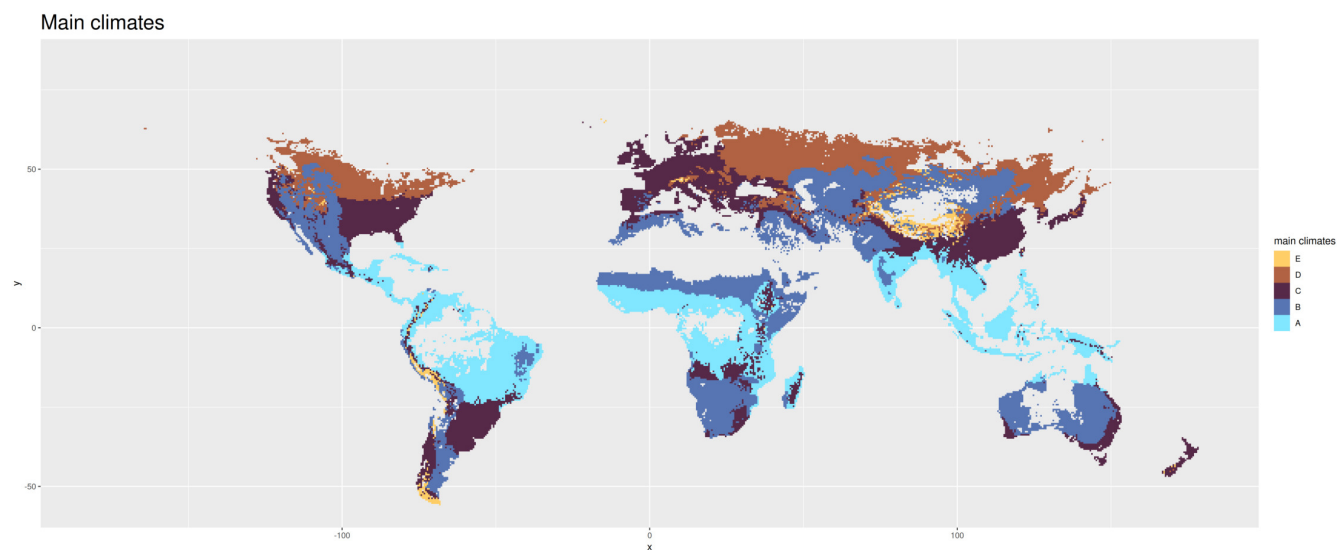


Figure A2. Main climates according to the Köppen Geiger climate classification (Kottek et al. (2017)). A = equatorial, B = arid, C = Warm Temperate, D = Snow, E = Polar.

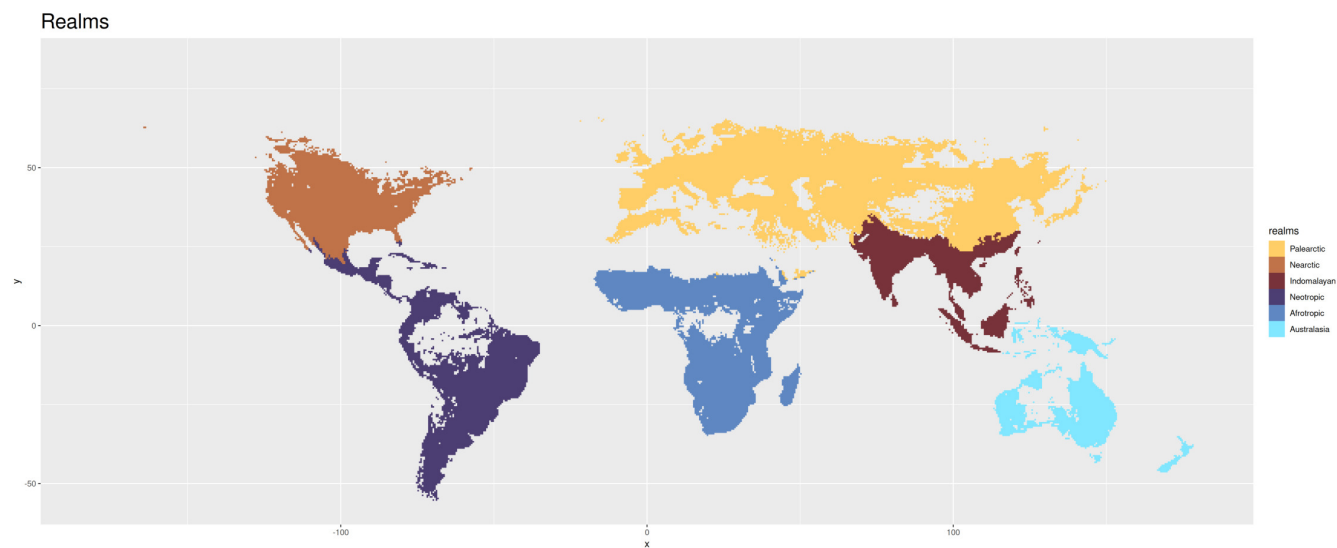


Figure A3. Biogeographic partition of the Earth into realms as defined in the Ecoregions framework (Dinerstein et al. (2017)).

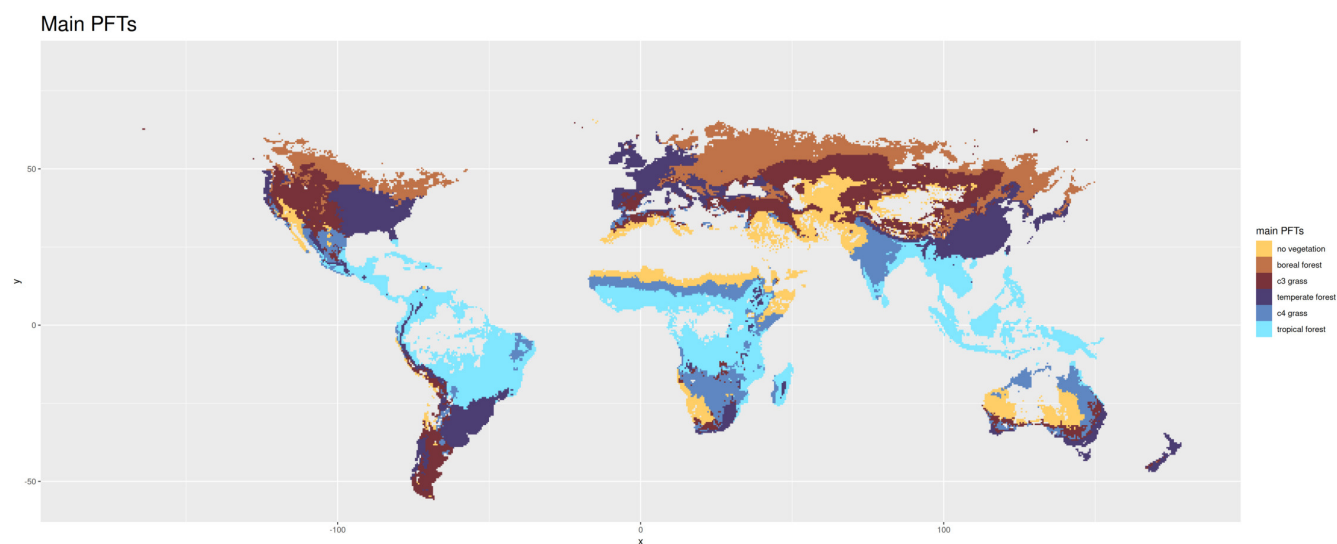


Figure A4. Classification based on main dominant plant functional types in LPJmL simulations without human-driven land use (see *Methods*). Tiles are classified as “noVeg” if they are predominantly not covered by any vegetation.

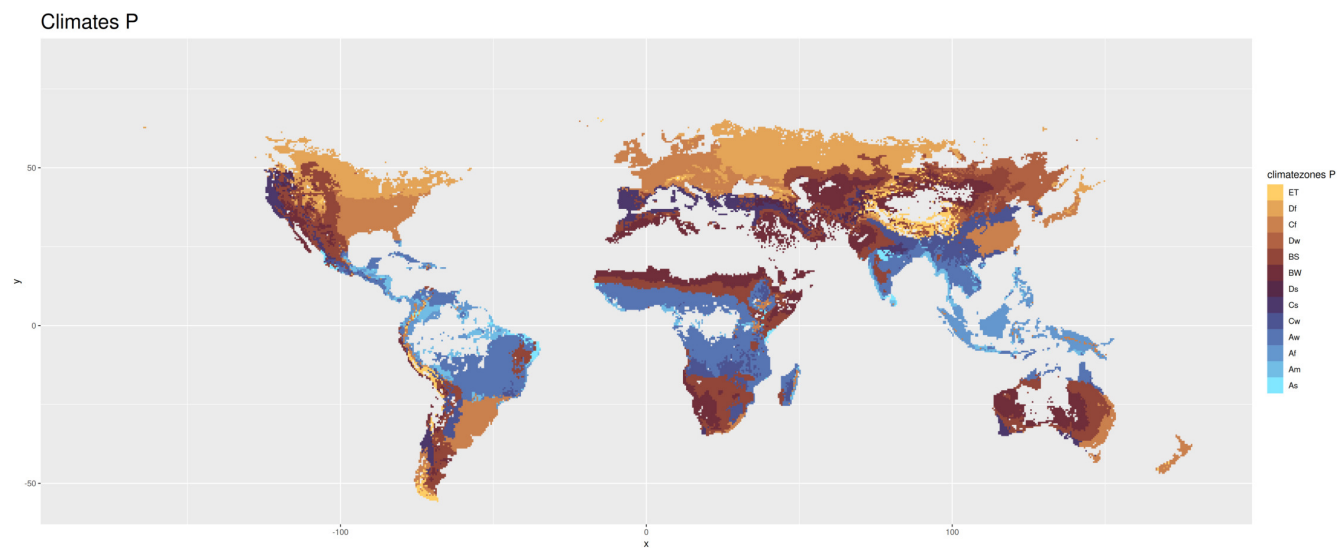


Figure A5. Main climate and precipitation types according to the Köppen Geiger climate classification scheme. See Appendix B for the nomenclature.

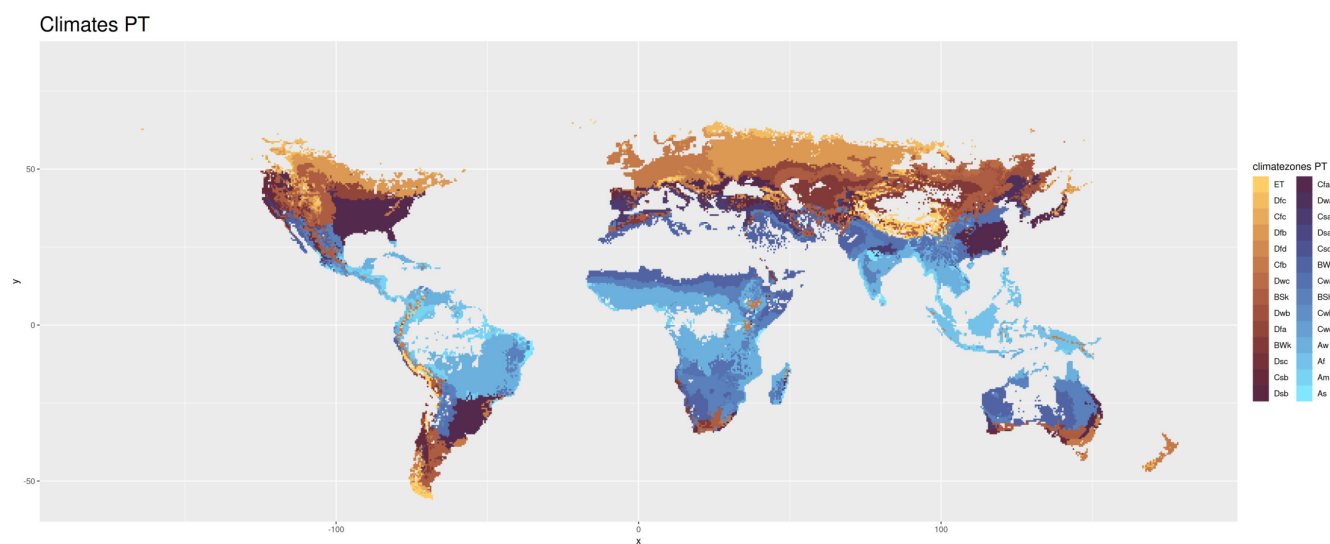


Figure A6. Climate zones according to the Köppen Geiger climate classification scheme. See Appendix B for the nomenclature.

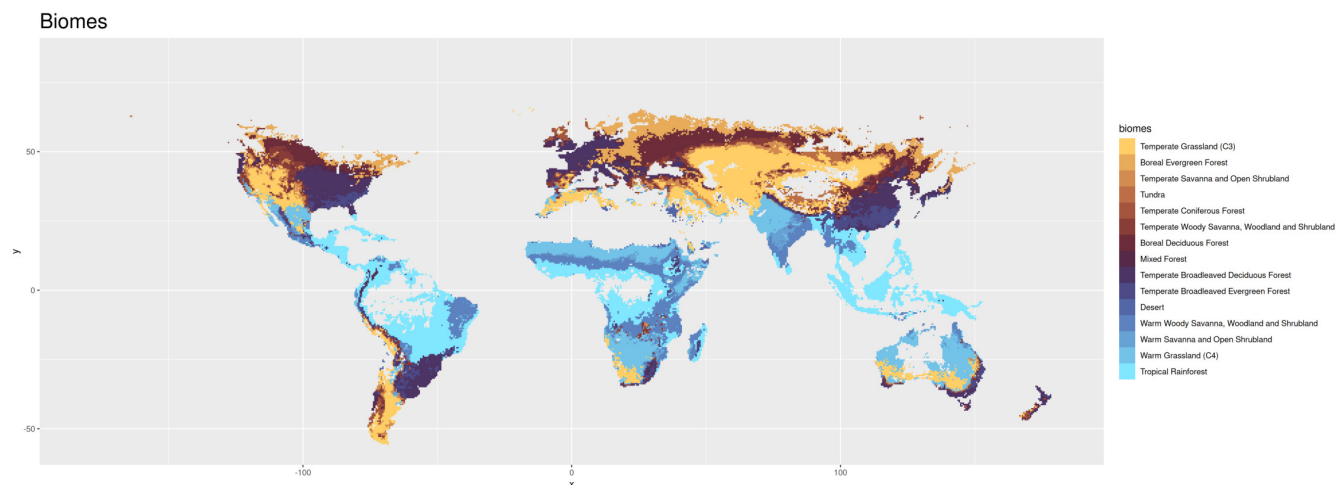


Figure A7. Biogeographic partition of the Earth into biomes according to the Ecoregions framework and identified via the Ostberg classification scheme (Ostberg et al. (2013), more recently used in Drüke et al. (2024)). This scheme is based on parameters produced by LPJmL – the foliar projective cover (FPC) of plant functional types (PFT) and vegetation carbon – to distinguish forests, savannas and shrublands, grasslands and deserts. Types of forests are further classified based on the dominant tree PFTs, while savannas and shrublands consider biomass limits as well as the fractions of trees vs. grasses. Grassland biomes include warm (C4-dominated) vs. temperate grasslands (C3-dominated). The tundra biome is determined using the temperature limits from the climate forcing dataset, the Climate Research Unit (CRU) gridded Time Series (TS) (Harris et al. (2014)). The classification is based on the LPJmL simulation without human-driven land use (compare *Methods*)

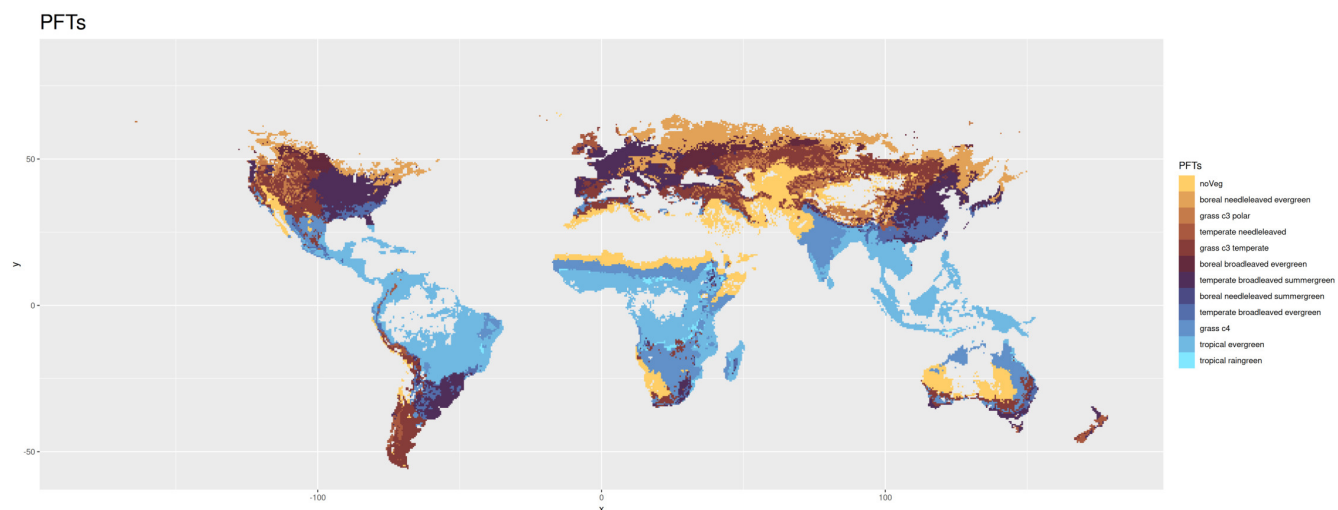


Figure A8. Classification into dominant plant functional types based on LPJmL simulations without human-driven land use (see *Methods*). Tiles are classified as “no vegetation” if they are predominantly not covered by any vegetation.

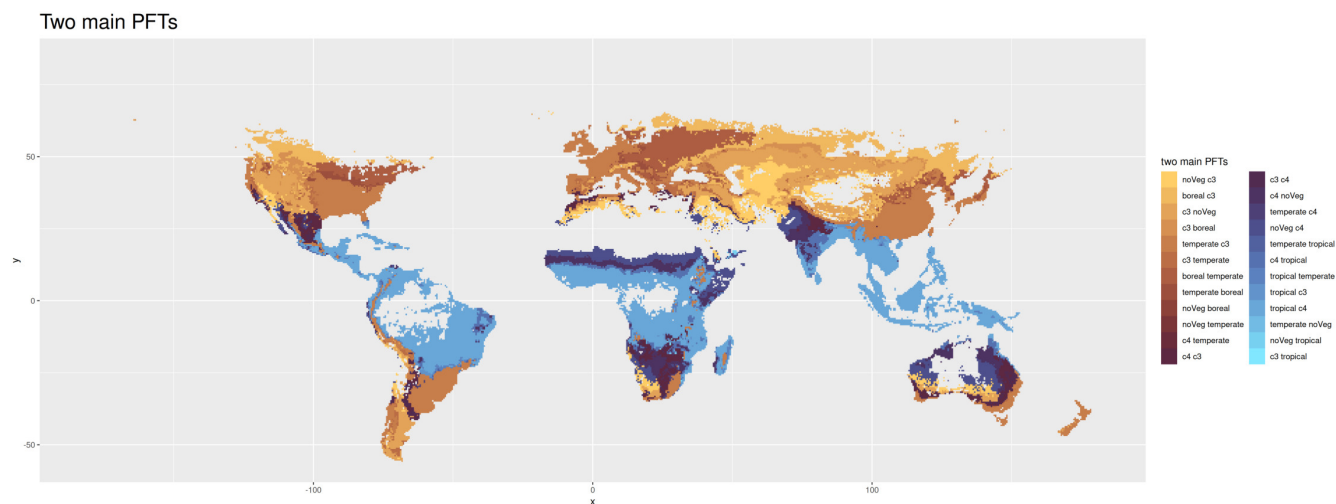


Figure A9. Classification based on the two dominant main plant functional types in LPJmL simulations without human-driven land use (see *Methods*). For the sake of readability, we omit “forest” after boreal, temperate, and tropical, and we omit “grass” after c3 and c4. We use “noVeg” as abbreviation for “no vegetation”. Tiles are classified as as “noVeg” if they are predominantly not covered by any vegetation.

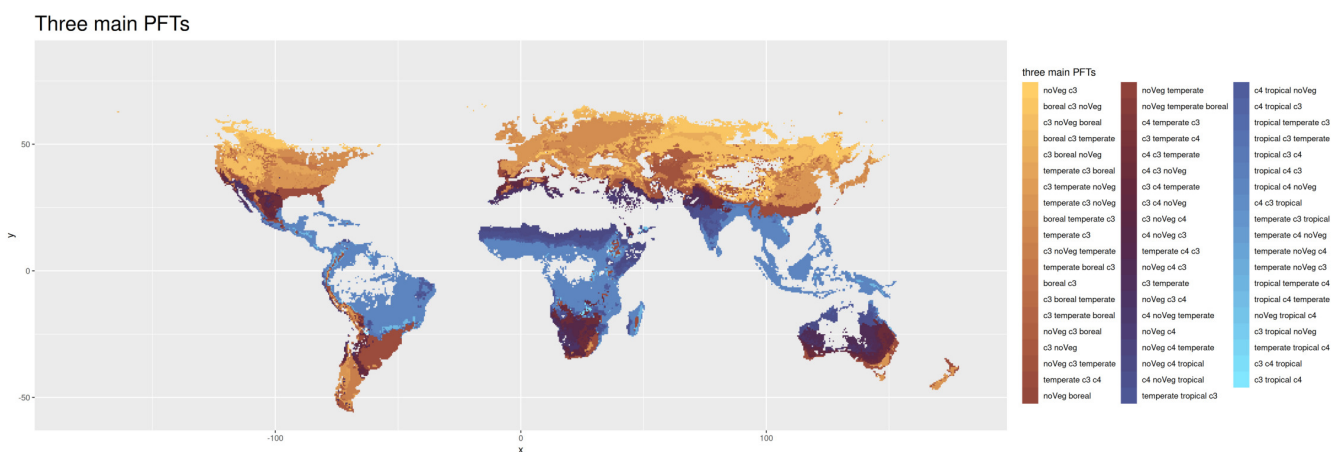


Figure A10. Classification based on the three dominant main plant functional types in LPJmL simulations without human-driven land use (see *Methods*). For the sake of readability, we omit “forest” after boreal, temperate, and tropical, and “grass” after c3 and c4. We use “noVeg” as abbreviation for “no vegetation”. Tiles are classified as “noVeg” if they are predominantly not covered by any vegetation.



Table B1. Köppen Geiger climate symbols

1st	2nd	3rd
A (Equatorial)	f (Rainforest, fully humid)	
	m (Monsoon)	
	s (Savannah with dry summer)	
	w (Savannah with dry winter)	
B (Arid)	W (Desert)	h (Hot)
	S (Steppe)	k (Cold)
C (Warm Temperate)	s (Dry summer)	a (Hot summer)
	w (Dry winter)	b (Warm summer)
	f (Fully humid)	c (Cool summer and cool winter)
		d (Extremely continental)
D (Snow)	s (Dry summer)	a (Hot summer)
	w (Dry winter)	b (Warm summer)
	f (Without dry season)	c (Cool summer and cool winter)
		d (Extremely continental)
E (Polar)	T (Tundra)	
	F (Frost)	

Explanation of the three-letter Köppen Geiger climate symbols. The first letter indicates the main climate, the second letter the precipitation conditions, and the third letter the temperature conditions. Adopted from Kottek et al. (2006).

Appendix B: Köppen Geiger classification scheme



385 **Appendix C: Spatially resolved maps of second-order impacts**

Our results reveal that a loss of natural vegetation cover driven by the change in human-induced land use causes an increase in surface water runoff in large parts of the world (Fig. 4A). This clear dominance of negative effect size (72 % of grid cells) can be traced back to the fact that deforestation typically leads to a decrease in the penetration of rainfall into the soil and thus to an increase in surface water runoff (Sterling et al. (2013)). This effect is especially strong in Asian c4 grasslands and in the Asian tropical forest, which, in undisturbed state, is characterized by a particularly high infiltration rate.

However, in some regions, we observe a slightly to moderately positive effect size, indicating that a decrease in natural vegetation cover leads to a decrease in surface water runoff. In central Australia, southern Africa, and the periphery of the Sahara desert, the most likely reason for this phenomenon is the increased evapotranspiration in these areas (Sterling et al. (2013)). Another factor might be a higher rainfall infiltration rate of cropland in comparison to the former barren soil. Moreover, we find positive effect size in temperate forest regions of Asia, Europe, North America, and South America.

While the transition from areas of negative to areas of positive effect size is typically gradual, it can be remarkably sharp, indicating hard transitions between ecosystems. In some cases, this is due to differences in altitude, such as for the Sichuan Basin in eastern Asia. In other cases, it reflects the distinctive features of river landscapes, such as in the lowland forests along the Mississippi river in eastern North America.

In contrast to the second-order impacts of land use change on runoff, we observe predominantly positive effect size in Fig. 4B (77 % of the grid cells), illustrating that in large parts of the world, a decrease in natural vegetation cover leads to a decrease in carbon dioxide uptake and storage. This effect is particularly high in the tropical forests of South America and Asia, due to their high vegetation content with its high carbon storage capacity (compare Lade et al. (2021b)). The formerly barren lands in central Australia, Asia, southern Africa, the peripheral Sahara desert, as well as in North America again display the opposite effect. This is likely due to the fact that the carbon storage capacity of cropland is higher than that of the formerly sparse vegetation.

The spatially resolved effects of climate change on water runoff and natural vegetation cover form more “patchy” patterns without a clear dominance in sign (Figs. 4C-D). This aligns with the high variability of effect size reported in Lade et al. (2021b), reflecting the complex responses to increasing levels of atmospheric carbon concentration (Zhou et al. (2023)). The effects of rising CO₂-levels include both *radiative* and *physiological* forcing. Radiative forcing directly influences precipitation, air temperature, and radiation. Changes in these climate variables can affect soil moisture and vegetation cover, crucial factors in the partitioning of precipitation into evapotranspiration and runoff. Physiological forcing described the vegetation’s physical responses to increasing levels of atmospheric CO₂, such as a reduction in stomatal conductance, which generally decreases transpiration, and an increase in vegetation cover, which typically increases transpiration (Piao et al. (2007)). Hence, a deeper understanding of the observed patterns of second-order impacts requires a regional assessment of this balance.

We find several hotspot of positive effect size between climate change and surface water runoff in the tropical forests of Asia, Australia, and South America. This aligns with Zhou et al.’s hypothesis that in the regions where vegetation cover is



already close to saturation, an increasing levels of atmospheric CO₂ mainly leads to a decrease in transpiration and thereby to an increase in runoff (Zhou et al. (2023)).

420 In accordance with Zhou et al., we find climate change-induced increases in vegetation cover in the western United States and on the Tibetan plateau in central Asia (marked by a positive effect size in Figs. 4D). This effect can be traced back to enhanced metabolism and extended growing seasons through warming. With respect to runoff, the increasing vegetation cover possibly sets off the effect of the observed increasing precipitation. Indeed, we find a strong decrease in runoff on the Tibetan plateau (marked by a negative effect size in 4C), and no significant effect of climate change on runoff in the western United
425 States.

In the boreal forests of Europe, we observe large areas of positive effect size between climate change and runoff. This aligns with Zhou et al.'s hypothesis that the decrease in soil moisture exceeds the effect of increasing vegetation cover in many boreal regions (Zhou et al. (2023)).



Appendix D: The BR index for top-down clustering by effect type

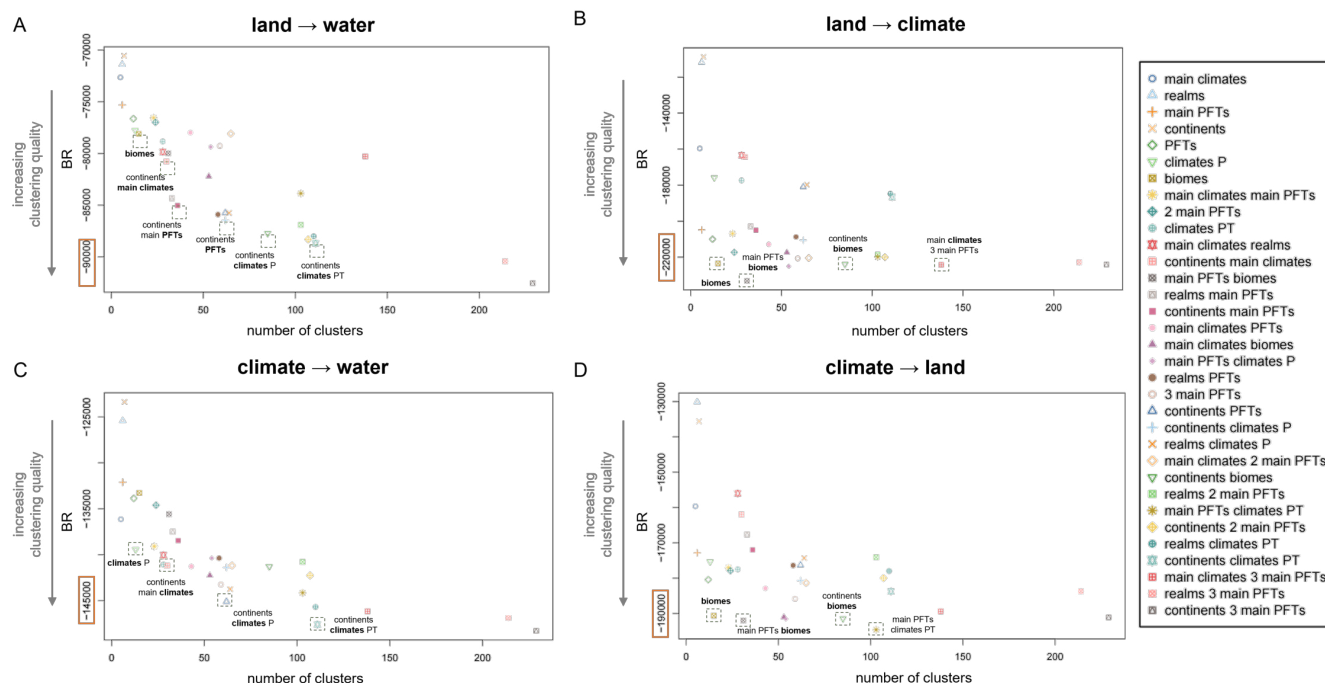


Figure D1. Within-cluster similarity of top-down partitions. Banfield-Raftery index (BR) of the 33 geographical, and biological Earth partitions with respect to the magnitude of the effects of natural vegetation cover on (A) surface water runoff and (B) carbon storage, as well as the magnitude of the effects of change in carbon dioxide concentration on (C) surface water runoff and (D) natural vegetation cover. The partitions are sorted by their number of clusters and highlighted if they stand out in performance compared to partitions of similar number of clusters.



430 Appendix E: Multivariate cluster validity indices for top-down clustering

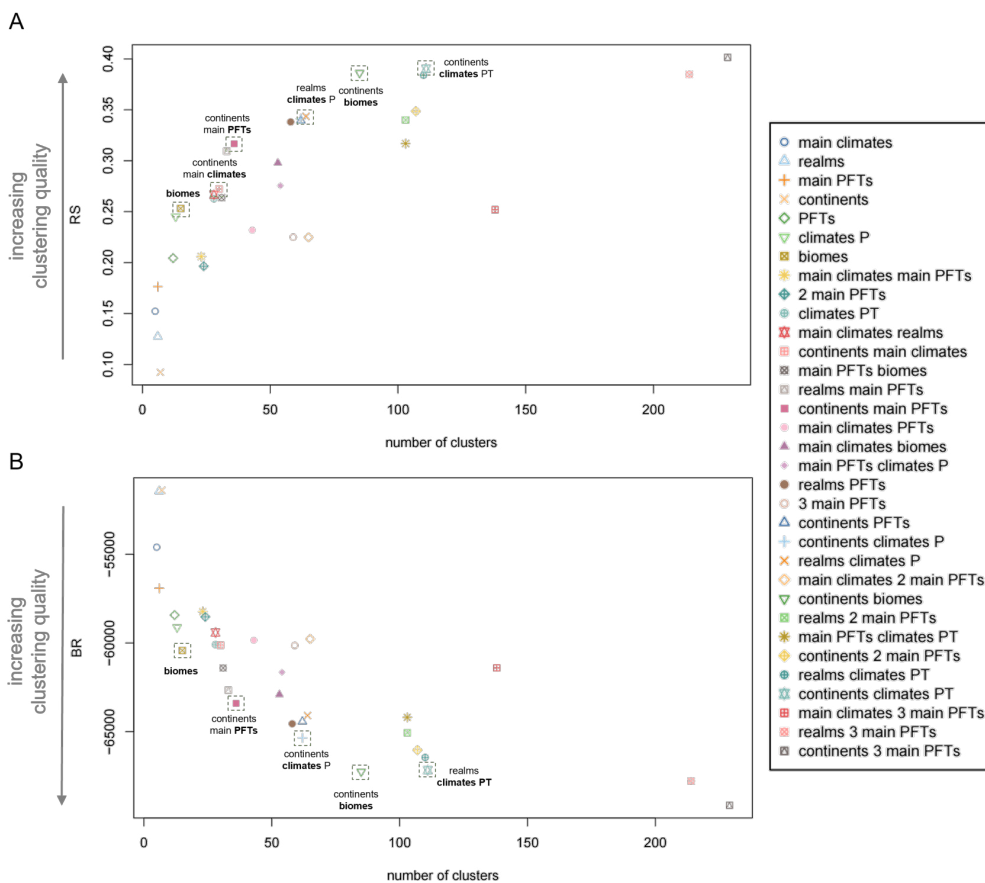


Figure E1. Multivariate clustering performance of top-down partitions. (A) R-squared index (RS) and (B) Banfield-Raftery index (BR) of the 33 geographical, climatic and biological Earth partitions with respect to the magnitude of the effects of natural vegetation cover on surface water runoff and carbon storage, as well as the magnitude of the effects of change in carbon dioxide concentration on surface water runoff and natural vegetation cover. The partitions are sorted by their number of clusters and highlighted if they stand out in performance compared to partitions of similar number of clusters.



Appendix F: Comparison of cluster validity indices for top-down and bottom-up clustering

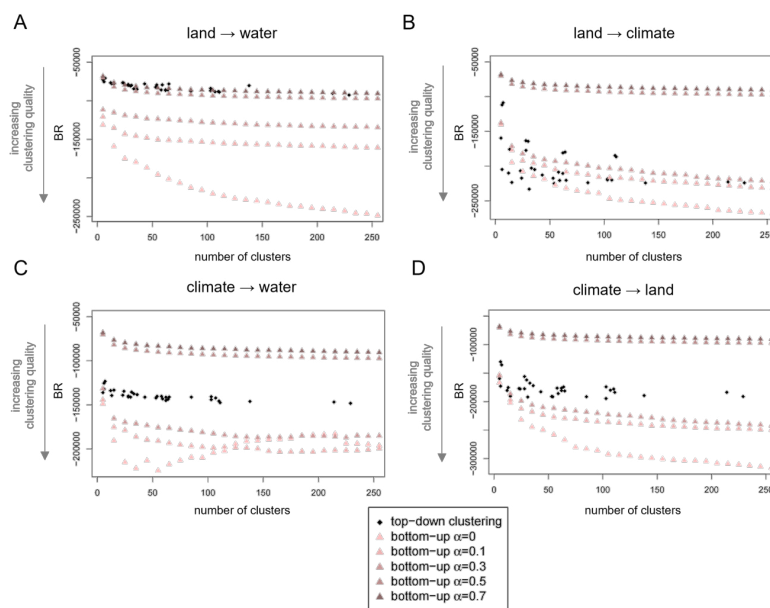


Figure F1. Comparison of clustering performance of top-down and bottom-up partitions. Banfield-Raftery index (BR) of the 33 “top-down” geographical, climatic and biological Earth partitions and of the GeoClust “bottom-up” neighborhood-based partitions without spatial constraints ($\alpha = 0$), and with mixing parameters $\alpha = 0.1, 0.3, 0.5, 0.7$. Performance is evaluated separately based on the one-dimensional feature space of magnitude for (A) the effect of land on water, (B) land on climate, (C) climate on water, and (D) climate on land, respectively. The partitions are sorted by their number of clusters.

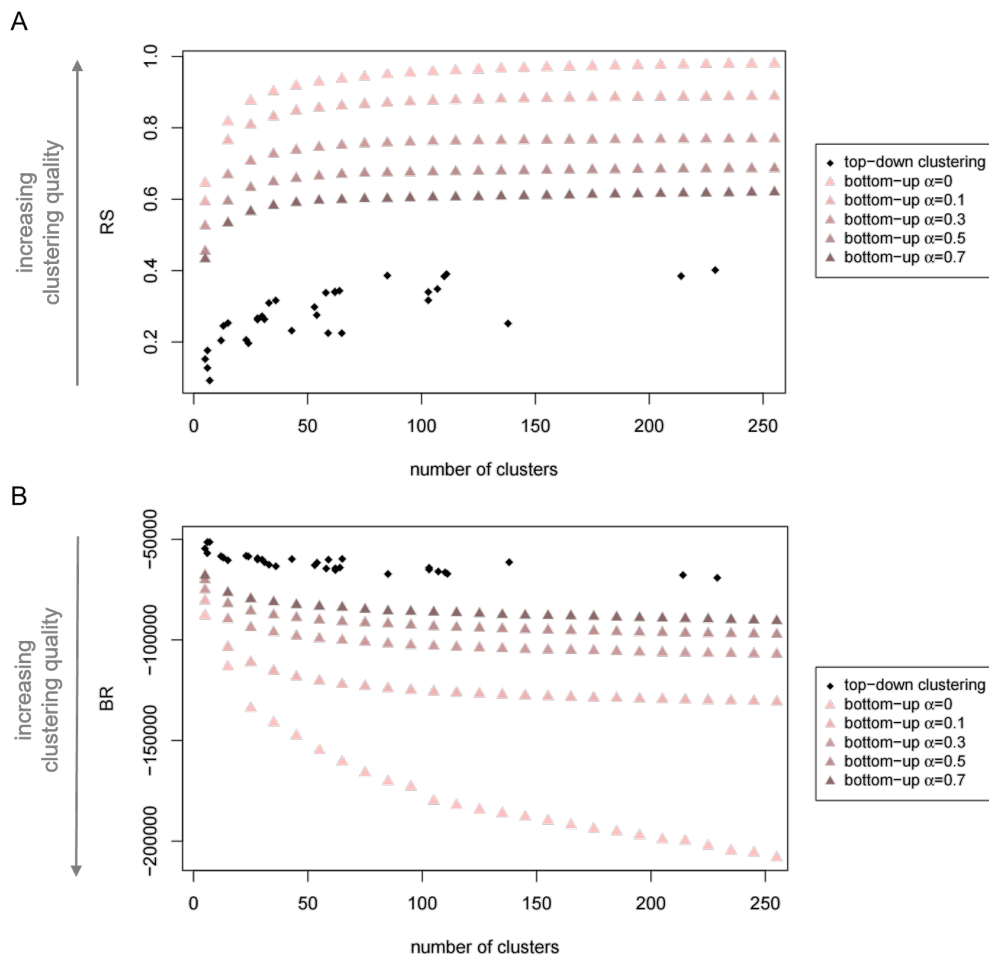


Figure F2. Comparison of multivariate clustering performance of top-down and bottom-up partitions. (A) R-squared index (RS) and (B) Banfield-Raftery index (BR) of the 33 “top-down” geographical, climatic and biological Earth partitions and of the GeoClust “bottom-up” neighborhood-based partitions without spatial constraints ($\alpha = 0$), and for mixing parameters $\alpha = 0.1, 0.3, 0.5, 0.7$. The four-dimensional feature space consists of the magnitudes of the effects of natural vegetation cover on surface water runoff and carbon storage, as well as the magnitudes of the effects of change in carbon dioxide concentration on surface water runoff and natural vegetation cover. The partitions are sorted by their number of clusters.



Appendix G: World maps of effects of climate change

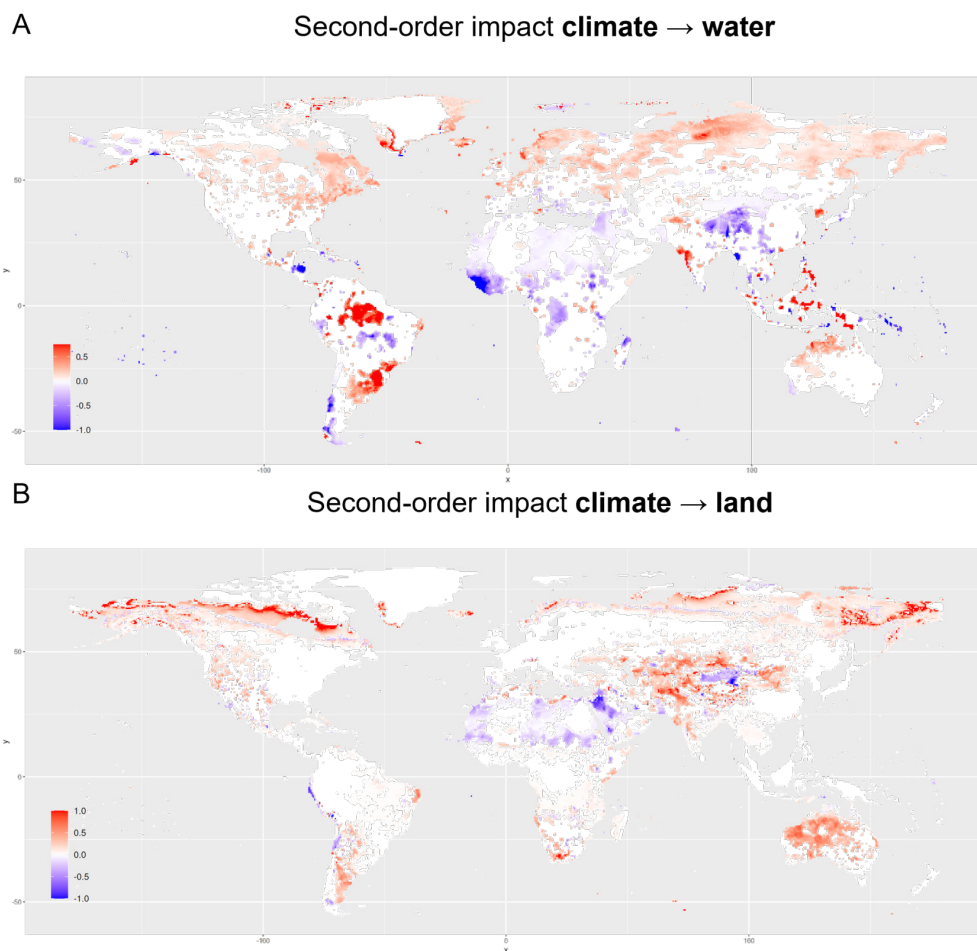
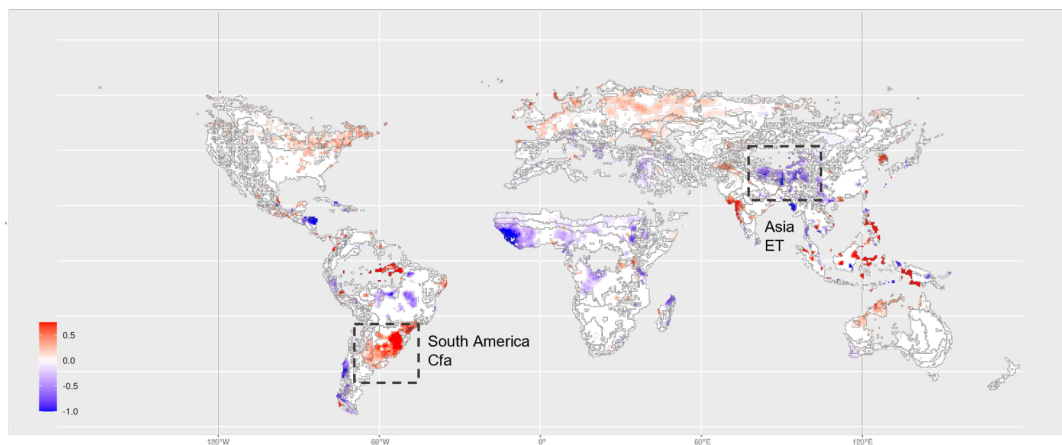


Figure G1. Global pattern of second-order impacts of climate change on water and land. The maps display the rescaled magnitudes of the effects of changes in carbon dioxide concentration on (A) surface water and (B) natural vegetation cover. Positive effect size indicates that an increase in carbon dioxide concentration causes an increase in the respective other Earth system process. Analogously, negative effect size indicates that an increase in carbon dioxide concentration leads to a decrease in the other process. Note that for the sake of visibility, the color scale varies across effect types and directions and should therefore not be used for cross-comparisons.



A

Partition “continents climates PT” on second-order impact **climate** → **water**



B

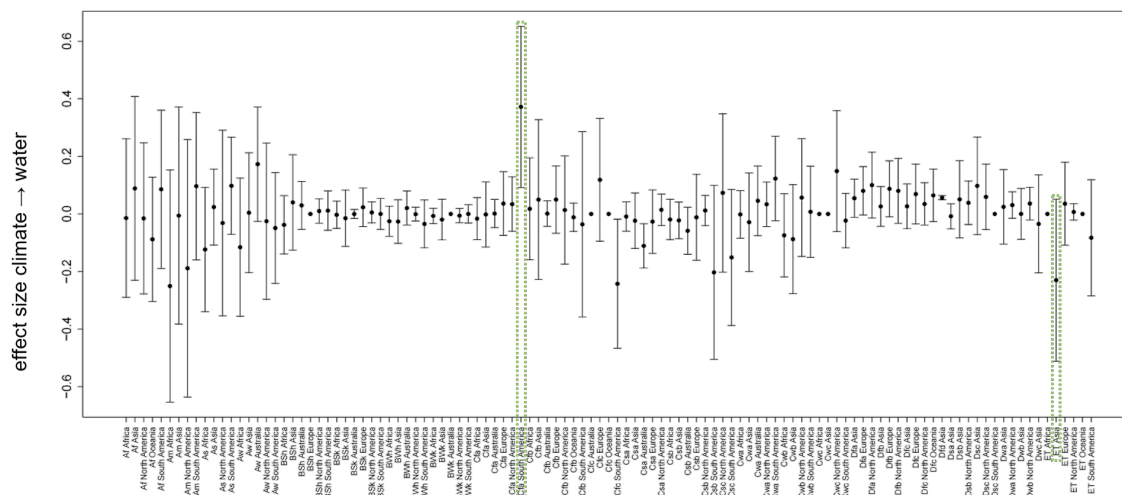
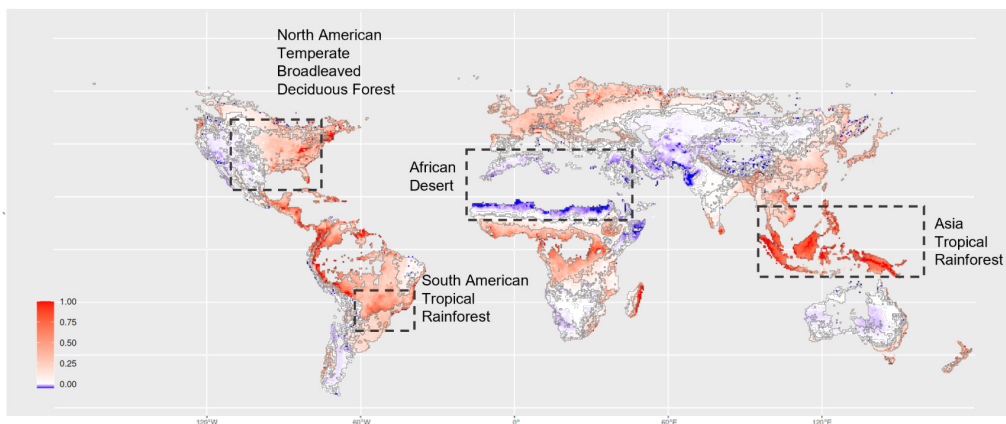


Figure H2. Magnitude of the second-order impact of climate change on water with boundaries given by continent and Köppen-Geiger climate zone (climate PT). (A) Map showing the magnitude of the effect of change in carbon dioxide concentration on surface water runoff. Boundaries mark both continents and climates/precipitation. Areas mentioned in the main text are highlighted. (B) Mean and standard deviations of the effect size within each cluster of the partition in (A). See Table B1 for the nomenclature of the climate zones. The same clusters are highlighted in panel (A) and panel (B).



A

Partition “continents biomes” on second-order impact land → climate



B

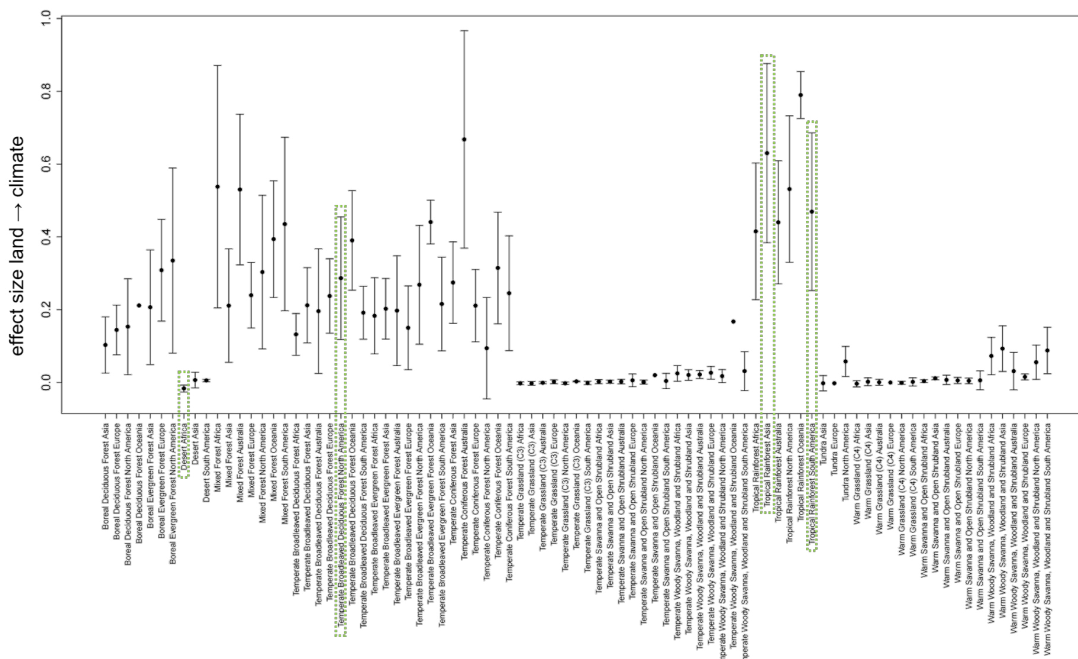
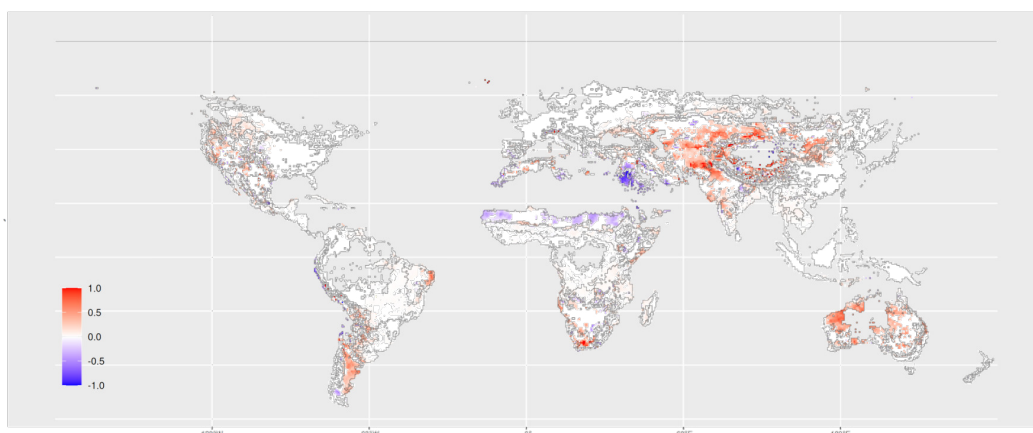


Figure H3. Magnitude of the second-order impact of land use change on climate with boundaries given by continent and biome. (A) Map showing the magnitude of the effect of change in natural vegetation cover on carbon dioxide storage. Boundaries mark both continents and biomes. Areas mentioned in the main text are highlighted. (B) Mean and standard deviations of the effect size within each cluster of the partition in (A). The same clusters are highlighted in panel (A) and panel (B).



A

Partition “continents biomes” on second-order impact climate → land



B

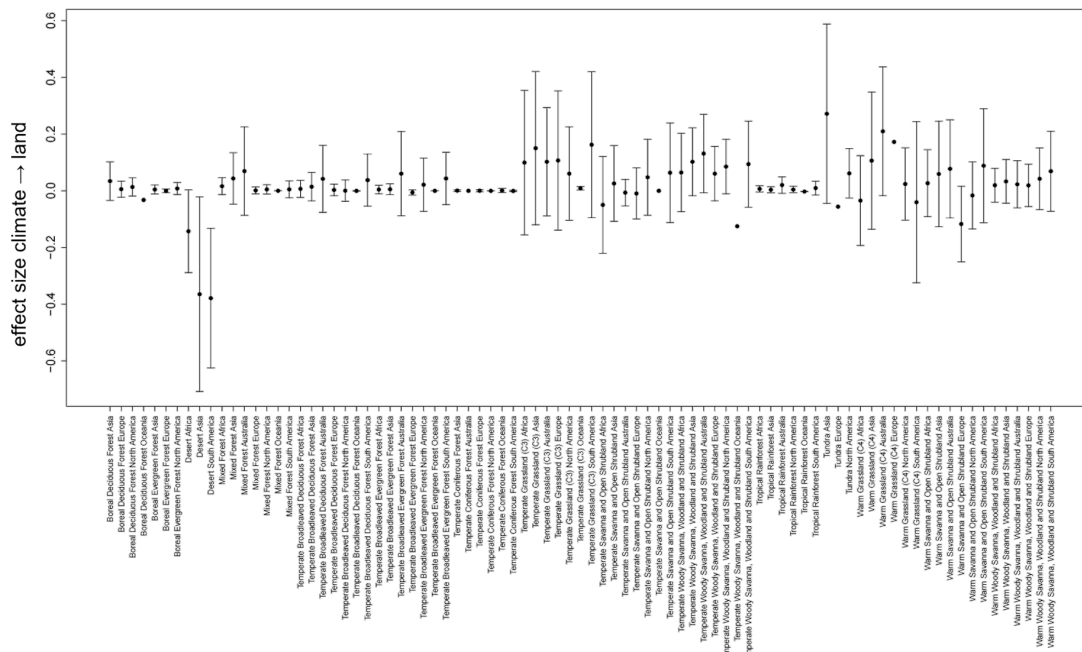


Figure H4. Magnitude of the second-order impact of climate change on natural vegetation cover with boundaries given by continent and the two main plant functional types (2 main PFTs). (A) Map showing the magnitude of the effect of change in carbon dioxide storage on natural vegetation cover. Boundaries mark both realms and the two main plant functional types. Areas mentioned in the main text are highlighted. (B) Mean and standard deviations of the effect size within each cluster of the partition in (A).



Appendix I: Aggregation of effect size by continent and main plant functional type

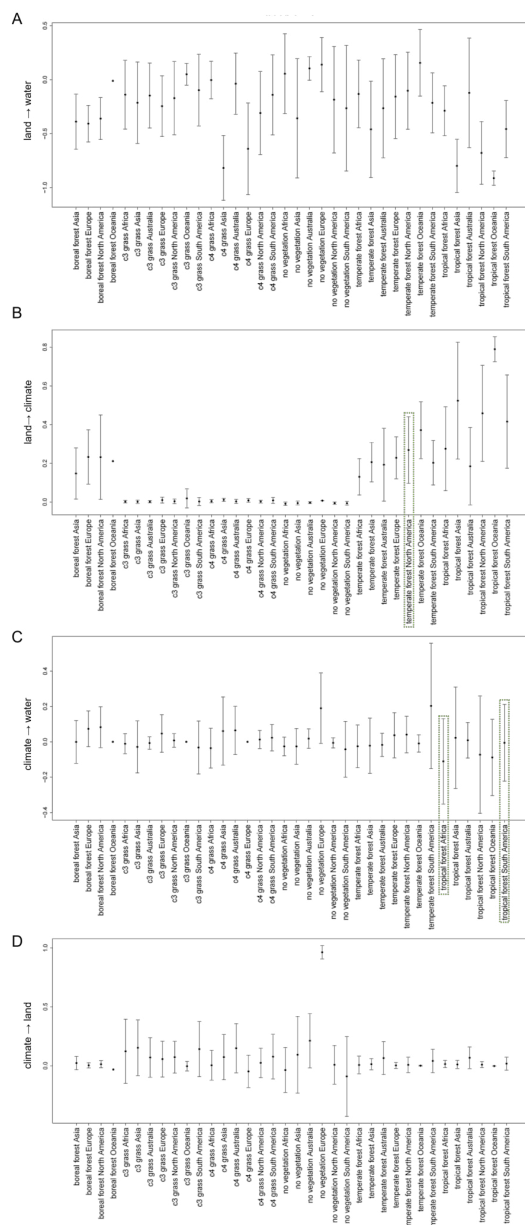


Figure 11. Aggregations of effect size with respect to the clusters used by Lade et al. (Lade et al. (2021b)). Clusters are based on a distinction of both continent and dominant main plant functional type. Mean and standard deviation of effect size within each cluster for the effects of land use change on (A) surface water runoff and on (B) climate, as well as for the effects of climate change on (C) surface water runoff and (D) natural vegetation cover. The highlighted clusters are being discussed in the Results and Discussion section.



435 Appendix J: Cluster validity indices for distance-based bottom-up clustering by effect type

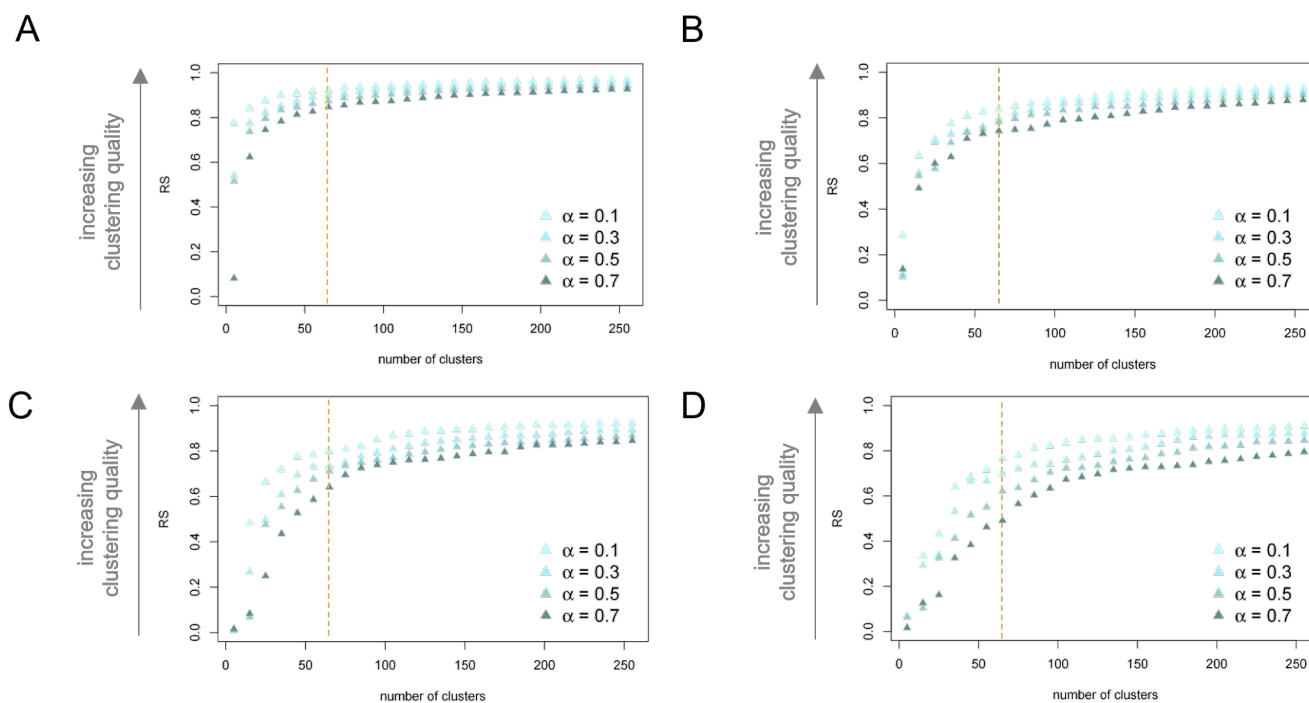


Figure J1. Performance of distance-based bottom-up partitions by effect type and for varying mixing parameter α . R-squared index (RS) for the distance-based bottom-up partition generated by ClustGeo based on the multidimensional feature space of the effects of natural vegetation change on (A) surface water runoff and (B) carbon dioxide storage as well as for the effects of change in carbon dioxide concentration on (C) surface water runoff and (D) natural vegetation cover. Indices are displayed for partitions generated with mixing parameter $\alpha = 0.1, 0.3, 0.5, 0.7$. Partitions are ordered by their number of clusters. The dashed orange lines mark indices for the partition into 65 clusters, which we consider in more detail.

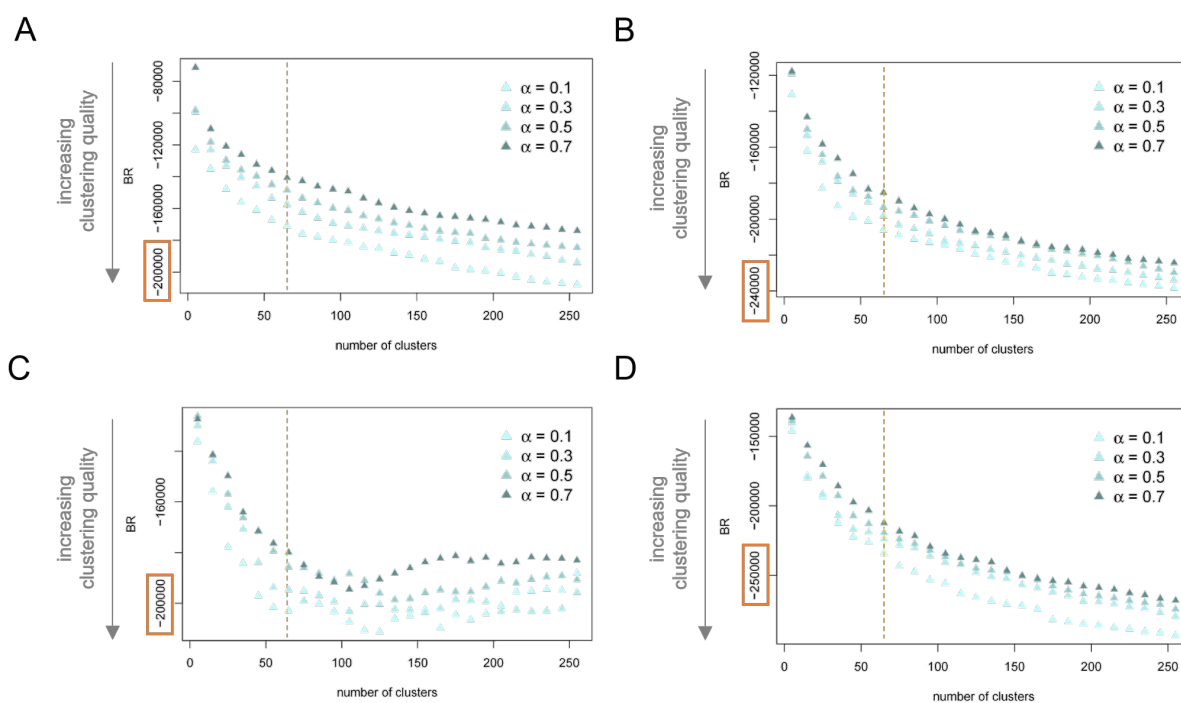


Figure J2. Performance of distance-based bottom-up partitions by effect type and for varying mixing parameter α . Banfield-Raftery index (BR) for the distance-based bottom-up partition generated by ClustGeo based on the multidimensional feature space of the effects of natural vegetation change on (A) surface water runoff and (B) carbon dioxide storage as well as for the effects of change in carbon dioxide concentration on (C) surface water runoff and (D) natural vegetation cover. Indices are displayed for partitions generated with mixing parameter $\alpha = 0.1, 0.3, 0.5, 0.7$. Partitions are ordered by their number of clusters. The dashed orange lines mark indices for the partition into 65 clusters, which we consider in more detail.



Appendix K: Distance-based bottom-up partitions for varying levels of spatial cohesion

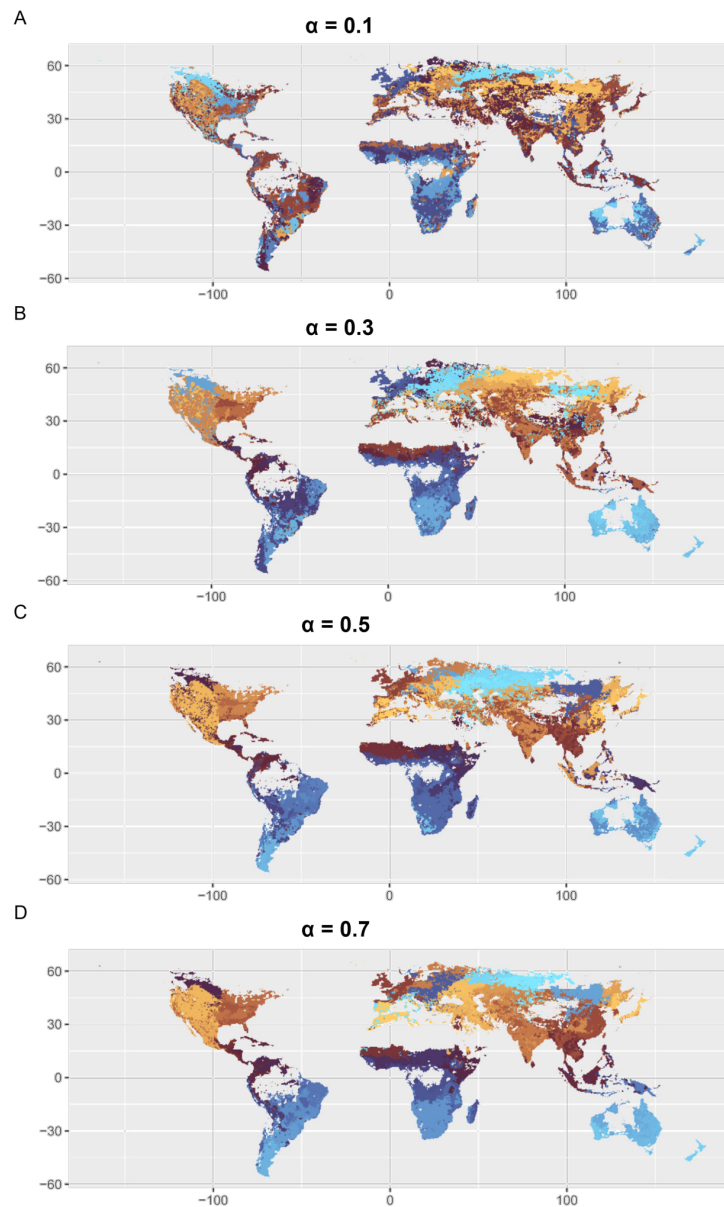


Figure K1. World map of bottom-up impact zones for increasing levels of spatial cohesion. Global pattern of 65 clusters based on a geographic-distance-based constraint space and the multidimensional feature space of magnitudes of the effects of land use change on water and climate and of the effects of climate change on water and land use. Generated via GeoClust with increasing level of spatial cohesion $\alpha = 0.1$ (A), $\alpha = 0.3$ (B), $\alpha = 0.5$ (C), $\alpha = 0.7$ (D).

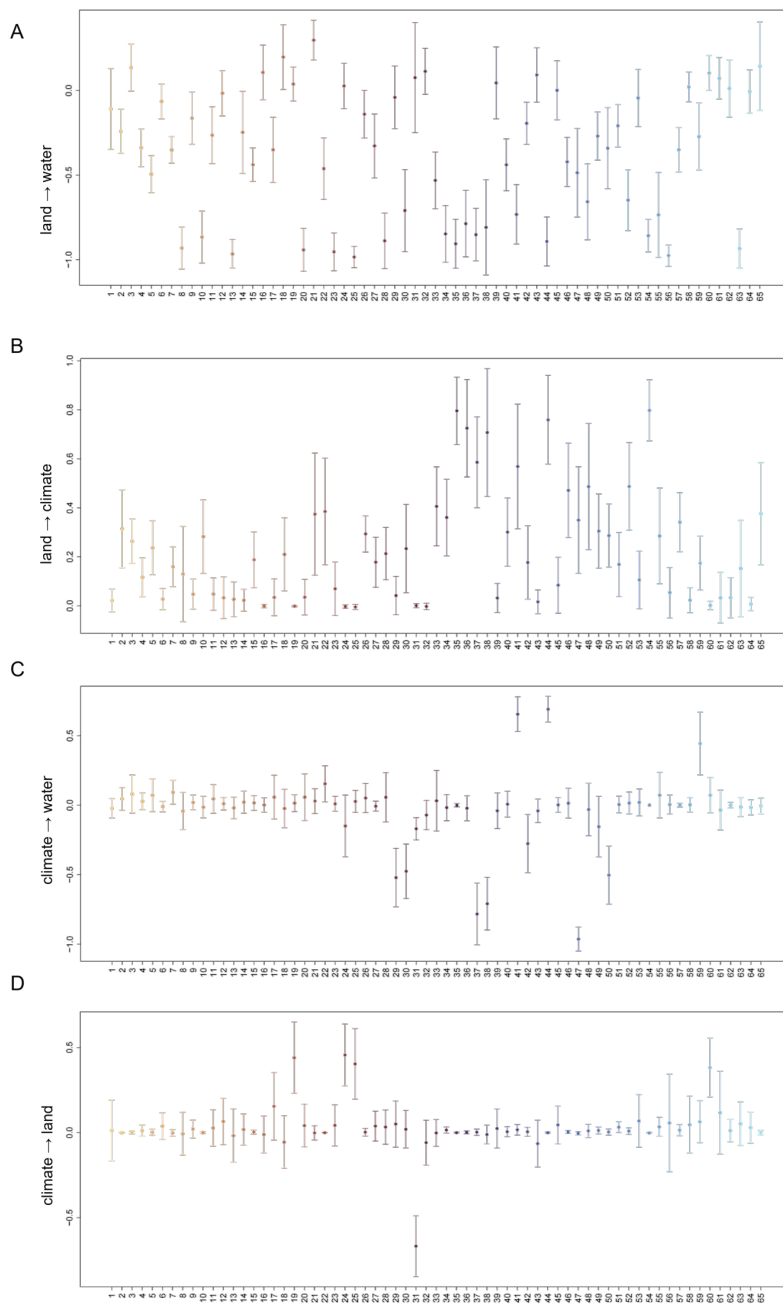


Figure K2. Mean and standard deviation of effect sizes in the bottom-up impact zones. The partition into $k = 65$ clusters was generated via GeoClust with mixing parameter $\alpha = 0.7$. Mean and standard deviation of effect sizes are displayed for the effects of land use change on (A) water and (B) climate and the effects of climate change on (C) water and (D) land use.



Appendix L: Sensitivity analysis: World maps of second-order impacts

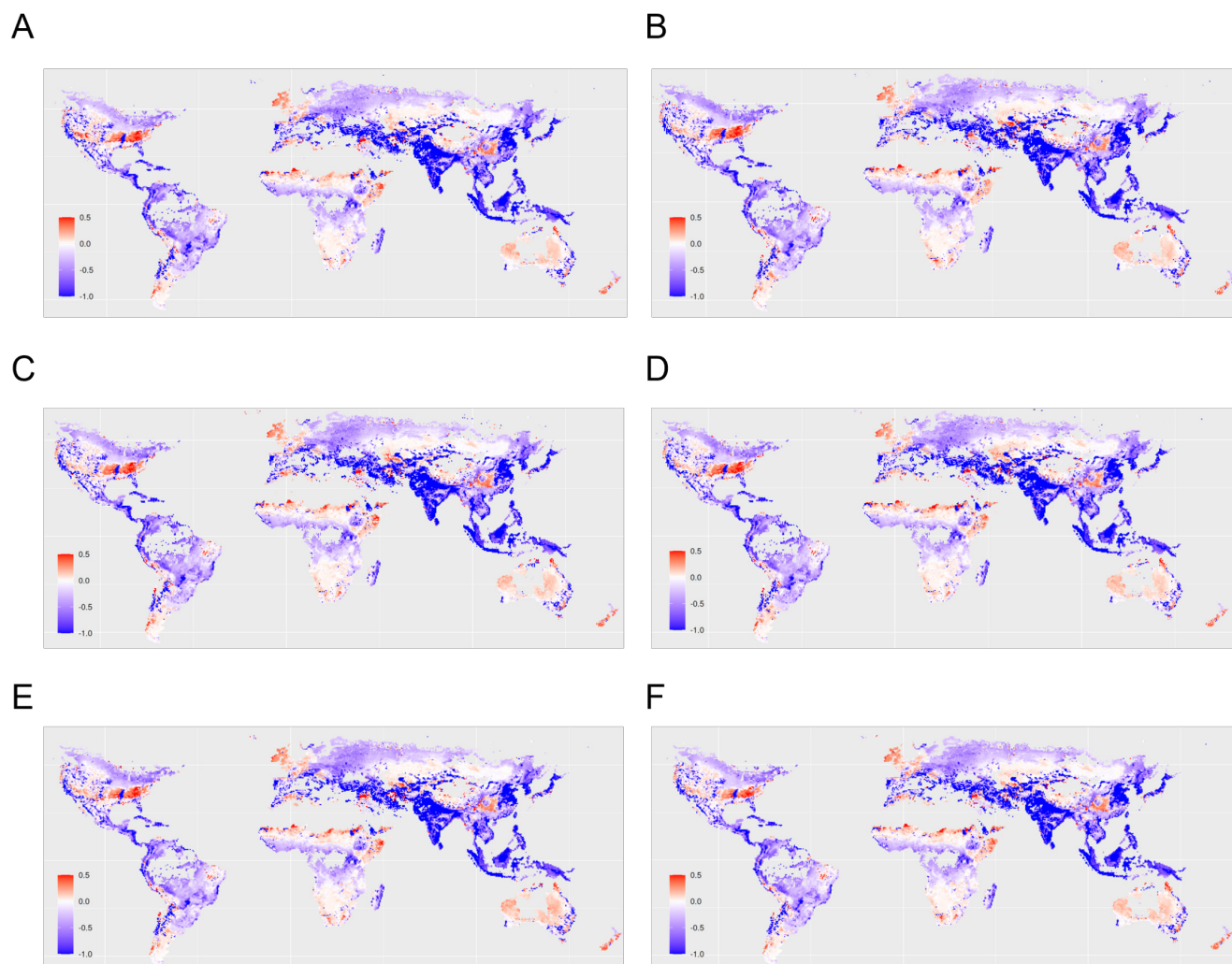


Figure L1. Sensitivity of the global pattern of second-order impacts of land use change on surface water runoff. The maps display outputs based on the climate model (A) HadGEM2-AO (B) GFDL-CM3 (C) NorESM1-ME (D) GFDL-ESM2G (E) CanESM2 (F) MIROC-ESM. Positive interaction strength (red) indicates that an increase in one Earth system process (e.g., increased natural vegetation cover) causes an increase in another Earth system process (e.g., increased surface water runoff). Analogously, negative effect size (blue) indicates that an increase in one process leads to a decrease in another process.

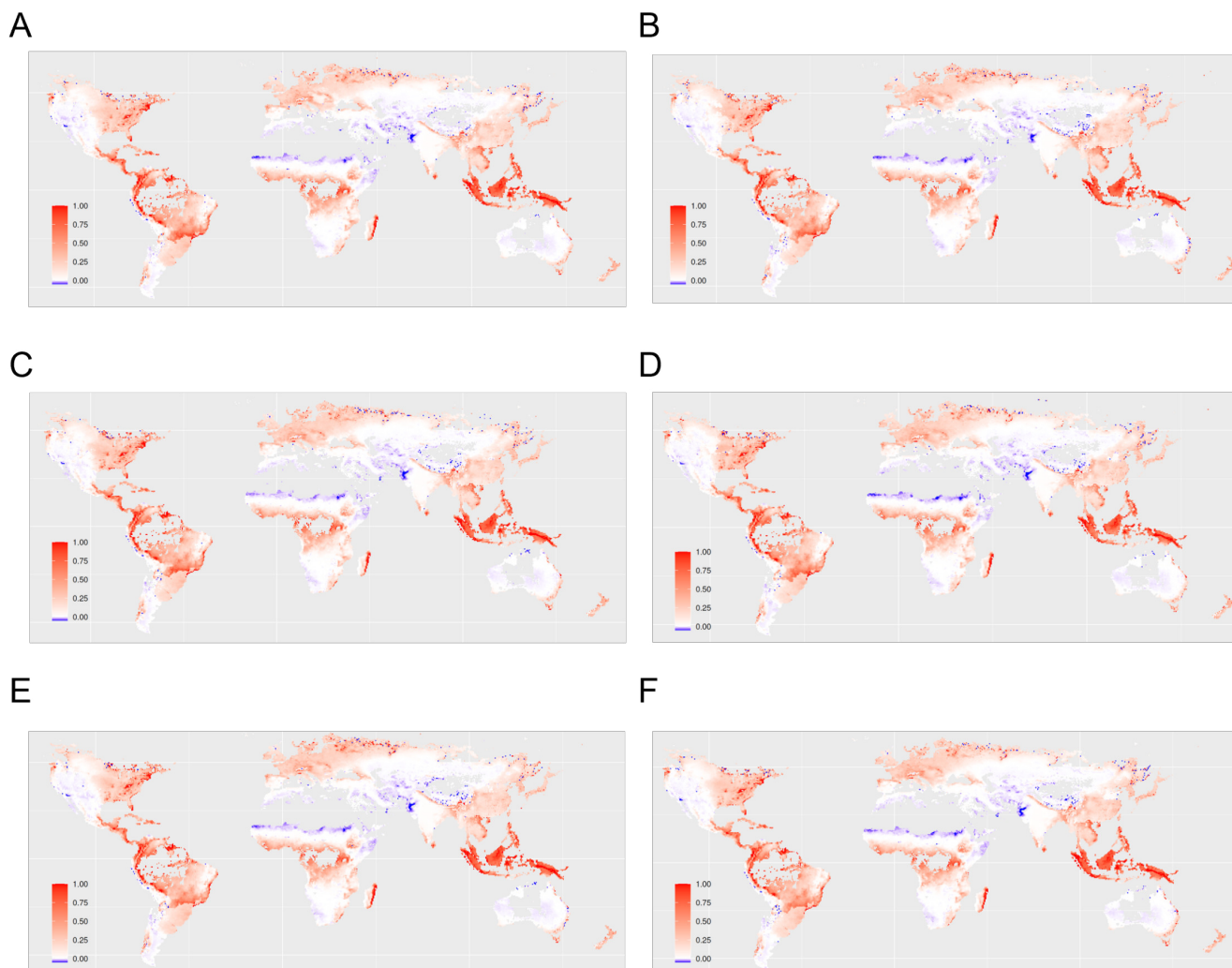


Figure L2. Sensitivity of the global pattern of second-order impacts of land use change on carbon storage density. The maps display outputs based on the climate model (A) HadGEM2-AO (B) GFDL-CM3 (C) NorESM1-ME (D) GFDL-ESM2G (E) CanESM2 (F) MIROC-ESM. Positive effect size (red) indicates that an increase in one Earth system process (e.g., increased natural vegetation cover) causes an increase in another Earth system process (e.g., increased surface water runoff). Analogously, negative effect size (blue) indicates that an increase in one process leads to a decrease in another process.

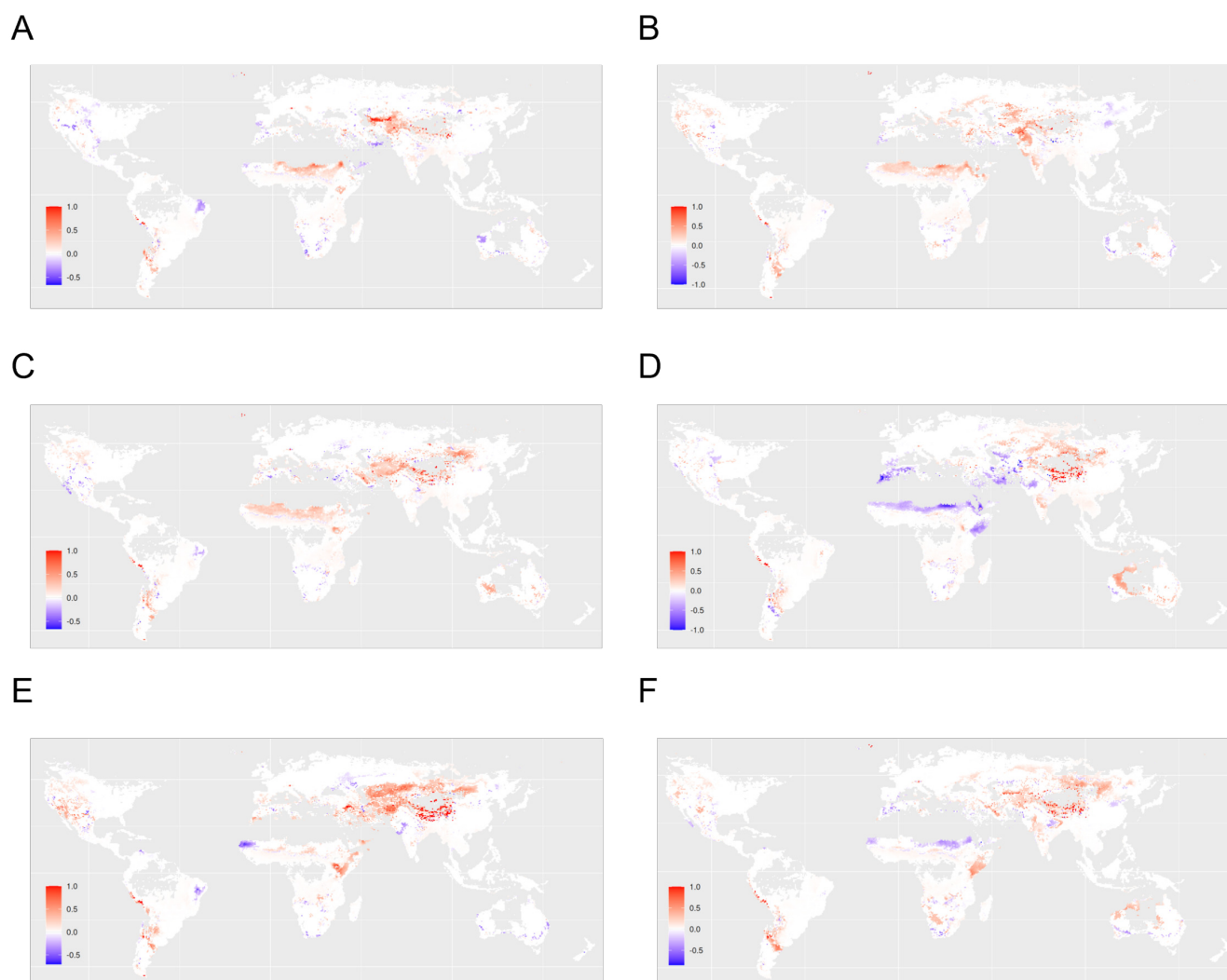


Figure L3. Sensitivity of the global pattern of second-order impacts of climate change on surface water runoff. The maps display outputs based on the climate model (A) HadGEM2-AO (B) GFDL-CM3 (C) NorESM1-ME (D) GFDL-ESM2G (E) CanESM2 (F) MIROC-ESM. Positive effect size (red) indicates that an increase in one Earth system process (e.g., increased natural vegetation cover) causes an increase in another Earth system process (e.g., increased surface water runoff). Analogously, negative effect size (blue) indicates that an increase in one process leads to a decrease in another process.

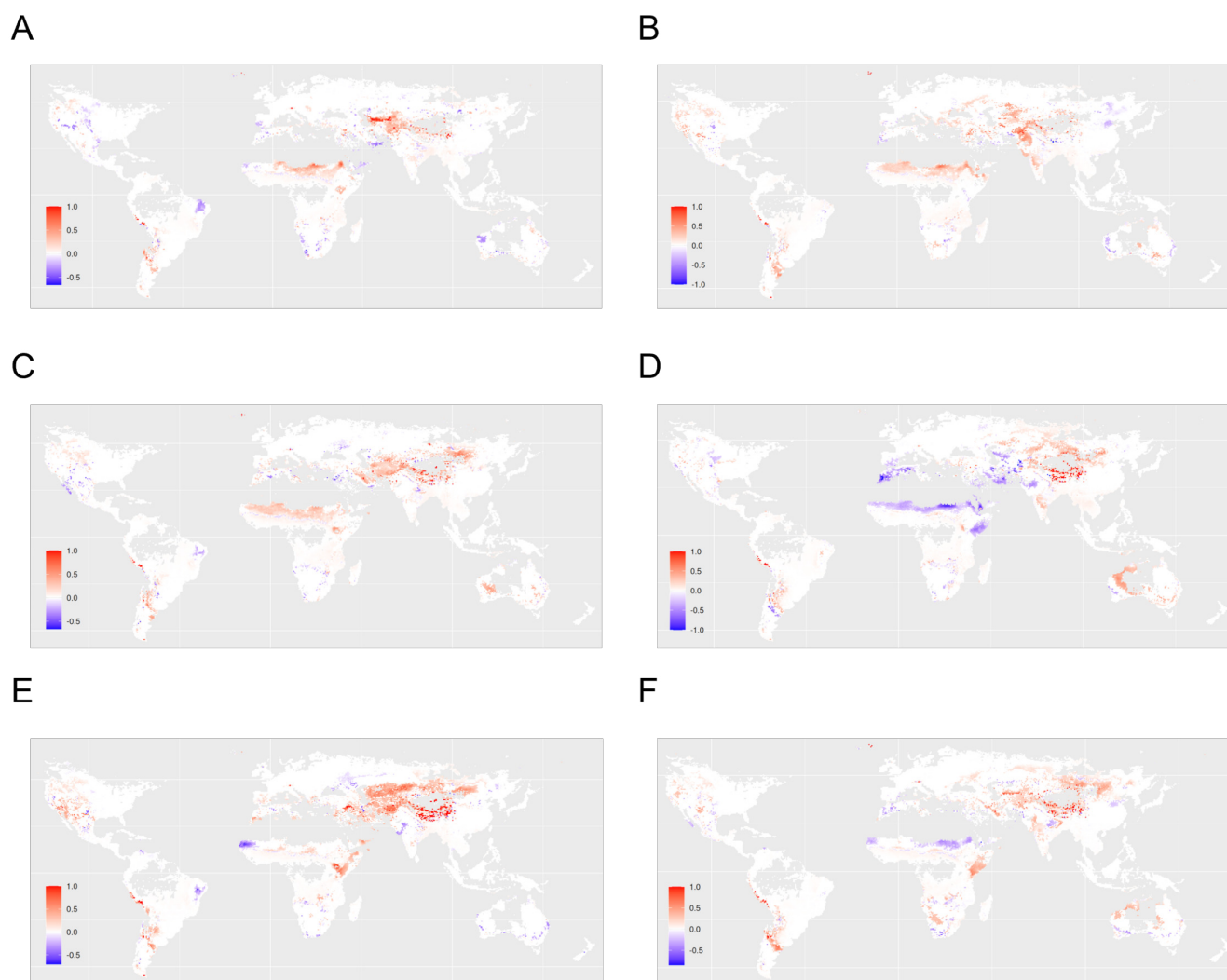


Figure L4. Sensitivity of the global pattern of second-order impacts of climate change on natural vegetation cover. The maps display outputs based on the climate model (A) HadGEM2-AO (B) GFDL-CM3 (C) NorESM1-ME (D) GFDL-ESM2G (E) CanESM2 (F) MIROC-ESM. Positive effect size (red) indicates that an increase in one Earth system process (e.g., increased natural vegetation cover) causes an increase in another Earth system process (e.g., increased surface water runoff). Analogously, negative effect size (blue) indicates that an increase in one process leads to a decrease in another process.



Appendix M: Sensitivity analysis: The RS index for top-down clustering by effect type

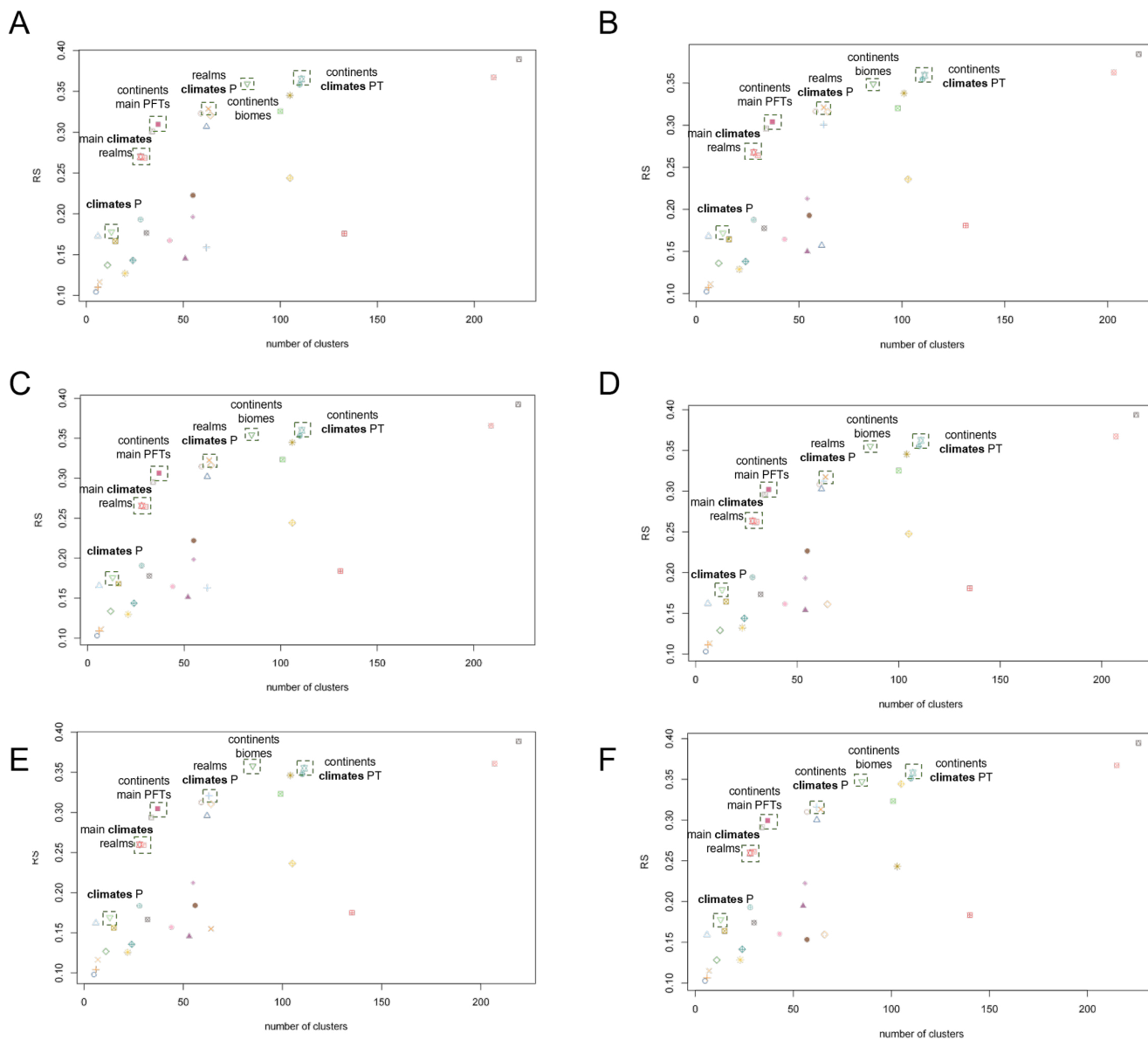


Figure M1. Sensitivity of the performance of the RS index for top-down clustering for the effect of land use change on surface water runoff. The maps display outputs based on the climate model (A) HadGEM2-AO (B) GFDL-CM3 (C) NorESM1-ME (D) GFDL-ESM2G (E) CanESM2 (F) MIROC-ESM. Positive effect size (red) indicates that an increase in one Earth system process (e.g., increased natural vegetation cover) causes an increase in another Earth system process (e.g., increased surface water runoff). Analogously, negative effect size (blue) indicates that an increase in one process leads to a decrease in another process.

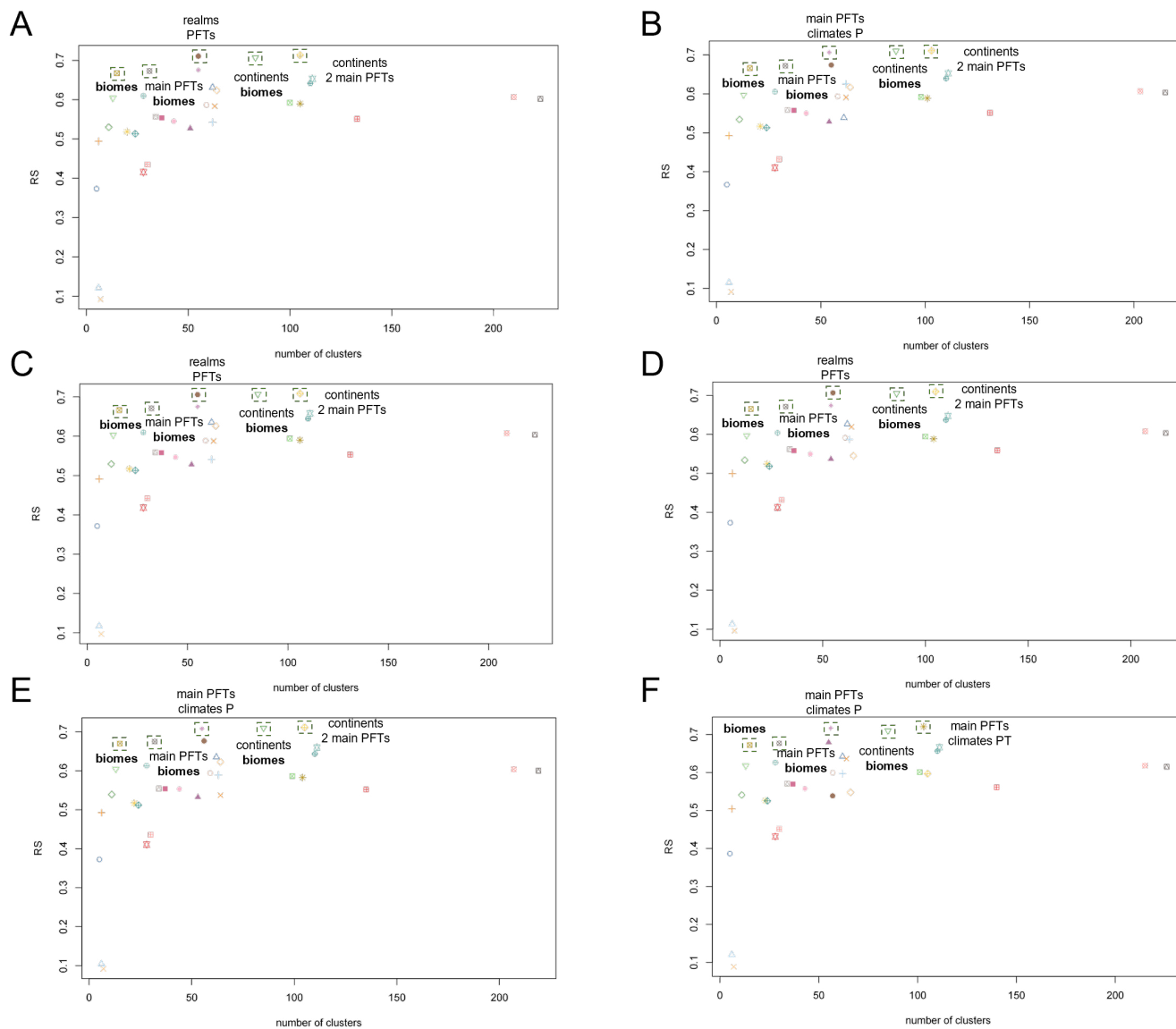


Figure M2. Sensitivity of the performance of the RS index for top-down clustering for the effect of land use change on carbon storage density. The maps display outputs based on the climate model (A) HadGEM2-AO (B) GFDL-CM3 (C) NorESM1-ME (D) GFDL-ESM2G (E) CanESM2 (F) MIROC-ESM. Positive effect size (red) indicates that an increase in one Earth system process (e.g., increased natural vegetation cover) causes an increase in another Earth system process (e.g., increased surface water runoff). Analogously, negative effect size (blue) indicates that an increase in one process leads to a decrease in another process.

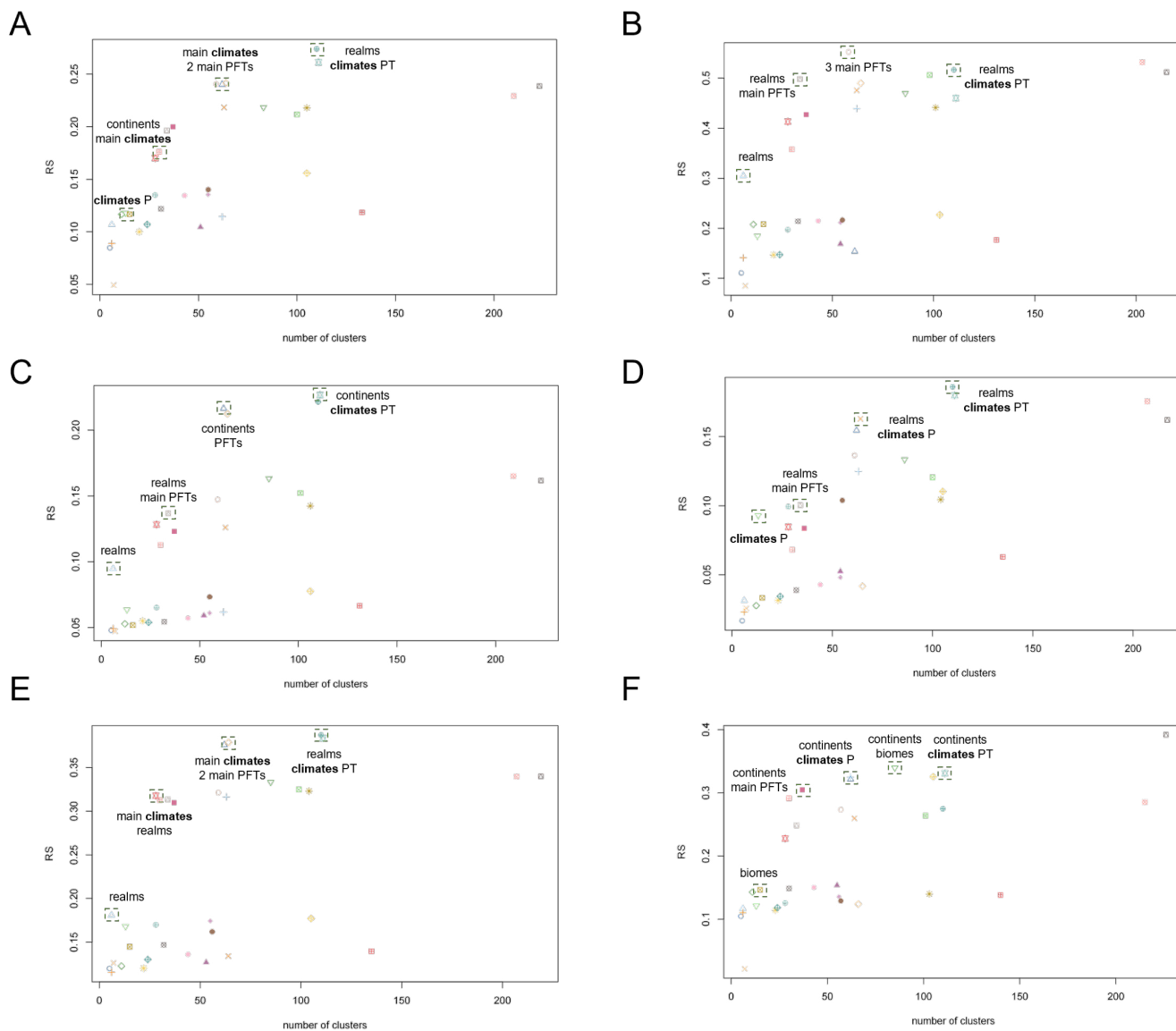


Figure M3. Sensitivity of the performance of the RS index for top-down clustering for the effect of climate change on surface water runoff. The maps display outputs based on the climate model (A) HadGEM2-AO (B) GFDL-CM3 (C) NorESM1-ME (D) GFDL-ESM2G (E) CanESM2 (F) MIROC-ESM. Positive effect size (red) indicates that an increase in one Earth system process (e.g., increased natural vegetation cover) causes an increase in another Earth system process (e.g., increased surface water runoff). Analogously, negative effect size (blue) indicates that an increase in one process leads to a decrease in another process.

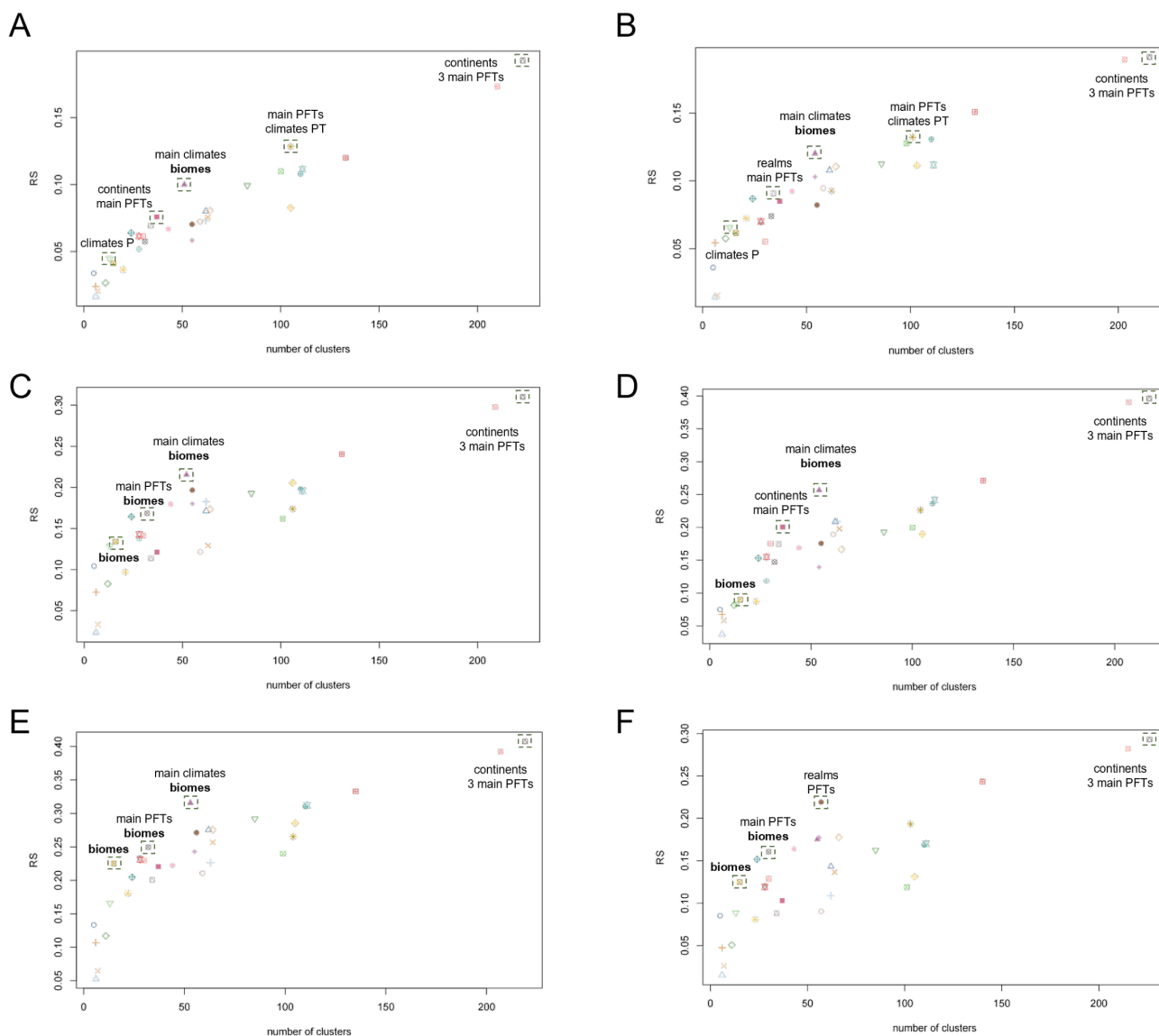


Figure M4. Sensitivity of the performance of the RS index for top-down clustering for the effect of land use change on surface water runoff. The maps display outputs based on the climate model (A) HadGEM2-AO (B) GFDL-CM3 (C) NorESM1-ME (D) GFDL-ESM2G (E) CanESM2 (F) MIROC-ESM. Positive effect size (red) indicates that an increase in one Earth system process (e.g., increased natural vegetation cover) causes an increase in another Earth system process (e.g., increased surface water runoff). Analogously, negative effect size (blue) indicates that an increase in one process leads to a decrease in another process.



Appendix N: Station coverage of the CRU TS3.21 dataset

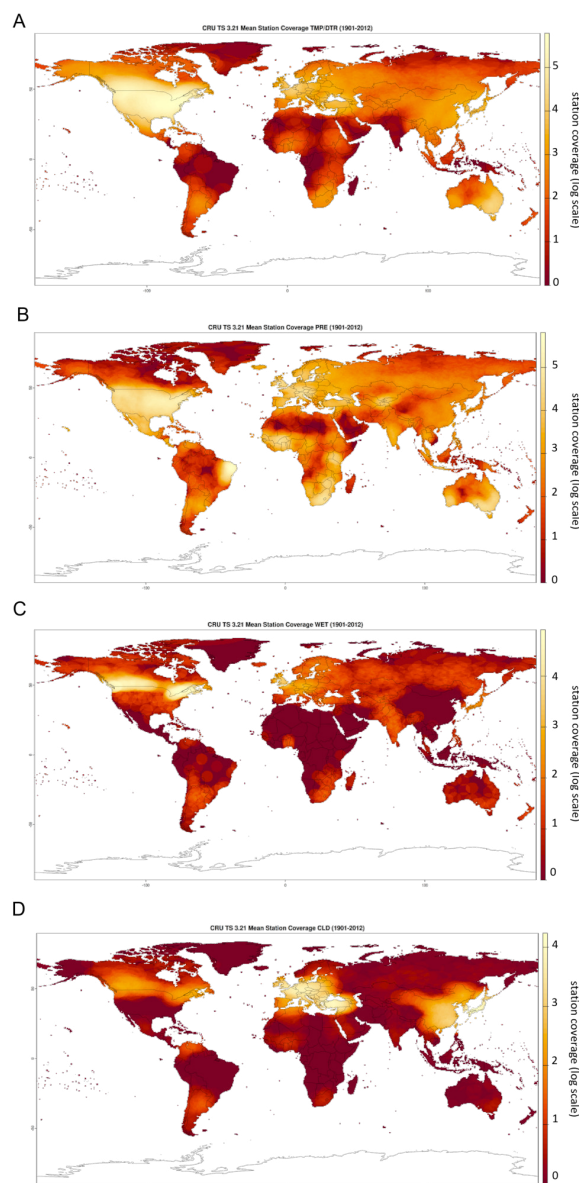


Figure N1. Station coverage underlying the CRU TS3.21 dataset (Harris (2013)). The station cover of a grid cell at a point in time is being defined as the number of stations within the correlation decay distance of the cell that were reporting a valid value at that point in time. Maps display the log-scaled station cover per grid cell averaged across 1901-2012 for the variables of (A) mean temperature (TMP) and diurnal temperature range (DTR) combined, (B) total precipitation (PRE), (C) rainday counts (WET) and (D) cloud cover (CLD). See Harris et al. (2014) for more details on the computation of the station coverage.



440 *Author contributions.* Conceptualization: HZ, SJL, JCR; Software: HZ, CKGG, IF, NC; Analysis: HZ, SJL, JCR, CKGG; Writing (original draft): HZ; Writing (revision): HZ, SJL, JCR, CKGG, IF, NC.

Competing interests. At least one of the (co-)authors serves as editor for the special issue to which this paper belongs.

Acknowledgements. HZ, JCR, IF, and NC received funding from the Swedish Research Council Formas (project 2023-00310). CKGG was funded by the Australian Government (Australian Research Council Discovery Project DP230101280). SJL was funded by the Australian
445 Government (Australian Research Council Future Fellowship FT200100381).



References

- Betts, R., Boucher, O., Collins, M., Cox, P., Falloon, P., Gedney, N., Hemming, D., Huntingford, C., Jones, C., Sexton, D., and Webb, M.: Projected Increase in Continental Runoff Due to Plant Responses to Increasing Carbon Dioxide, *Nature*, 448, 1037–41, <https://doi.org/10.1038/nature06045>, 2007.
- 450 Chavent, M., Kuentz-Simonet, V., Labenne, A., and Saracco, J.: ClustGeo: an R package for hierarchical clustering with spatial constraints, *Computational Statistics*, 33, 1799–1822, <https://doi.org/10.1007/s00180-018-0791-1>, 2018.
- Cramer, W., Bondeau, A., Woodward, I., Prentice, I., Betts, R., Brovkin, V., Cox, P., Fisher, V., Foley, J., Friend, A., Kucharik, C., Lomas, M., Ramankutty, N., Sitch, S., Smith, B., White, A., and Young-Molling, C.: Global response of terrestrial ecosystem structure and function to CO₂ and climate change: Results from six dynamic global vegetation models, *Global Change Biology*, 7, 357 – 373, <https://doi.org/10.1046/j.1365-2486.2001.00383.x>, 2001.
- 455 Dinerstein, E., Olson, D. P., Graham, D. J., Webster, A. L., Primm, S. A., Bookbinder, M. P., and Ledec, G. C.: A Conservation Assessment of the Terrestrial Ecoregions of Latin America and the Caribbean, *Environmental Conservation*, 23, 378 – 379, <https://api.semanticscholar.org/CorpusID:131043914>, 1995.
- Dinerstein, E., Olson, D., Joshi, A., Vynne, C., Burgess, N. D., Wikramanayake, E., Hahn, N., Palminteri, S., Hedao, P., Noss, R., Hansen, M., Locke, H., Ellis, E. C., Jones, B., Barber, C. V., Hayes, R., Kormos, C., Martin, V., Crist, E., Sechrest, W., Price, L., Baillie, J. E. M., Weeden, D., Suckling, K., Davis, C., Sizer, N., Moore, R., Thau, D., Birch, T., Potapov, P., Turubanova, S., Tyukavina, A., de Souza, N., Pinteá, L., Brito, J. C., Llewellyn, O. A., Miller, A. G., Patzelt, A., Ghazanfar, S. A., Timberlake, J., Klöser, H., Shennan-Farpón, Y., Kindt, R., Lillesø, J.-P. B., van Breugel, P., Graudal, L., Vogé, M., Al-Shammari, K. F., and Saleem, M.: Ecoregions2017 ^{©Resolve}, <https://ecoregions.appspot.com/>, accessed: 2025-02-28, 2017.
- 465 Drüke, M., Lucht, W., von Bloh, W., Petri, S., Sakschewski, B., Tobian, A., Loriani, S., Schaphoff, S., Feulner, G., and Thonicke, K.: The long-term impact of transgressing planetary boundaries on biophysical atmosphere–land interactions, *Earth System Dynamics*, 15, 467–483, <https://doi.org/10.5194/esd-15-467-2024>, 2024.
- Gupta, J., Bai, X., and Liverman, D. e. a.: A just world on a safe planet: a Lancet Planetary Health–Earth Commission report on Earth-system boundaries, translations, and transformations, *The Lancet Planetary Health*, 8, 2024.
- 470 Harris, I.: CRU TS3.21: Climatic Research Unit (CRU) Time-Series (TS) Version 3.21 of High Resolution Gridded Data of Month-by-month Variation in Climate (Jan. 1901 - Dec. 2012), <https://doi.org/10.5285/D0E1585D-3417-485F-87AE-4FCECF10A992>, accessed: 2025-12-19, 2013.
- Harris, I., Jones, P., Osborn, T., and Lister, D.: Updated high-resolution grids of monthly climatic observations – the CRU TS3.10 Dataset, *International Journal of Climatology*, 34, 623–642, <https://doi.org/https://doi.org/10.1002/joc.3711>, 2014.
- 475 Ito, A. and Inatomi, M.: Water-Use Efficiency of the Terrestrial Biosphere: A Model Analysis Focusing on Interactions between the Global Carbon and Water Cycles, *Journal of Hydrometeorology*, 13, 681–694, <https://doi.org/10.1175/JHM-D-10-05034.1>, 2012.
- Jong, R., Schaepman, M., Furrer, R., de Bruin, S., and Verburg, P.: Spatial relationship between climatologies and changes in global vegetation activity, *Global change biology*, 19, <https://doi.org/10.1111/gcb.12193>, 2013.
- Koirala, S., Jung, M., Reichstein, M., de Graaf, I. E. M., Camps-Valls, G., Ichii, K., Papale, D., Ráduly, B., Schwalm, C. R., Tramontana, G., and Carvalhais, N.: Global distribution of groundwater-vegetation spatial covariation, *Geophysical Research Letters*, 44, 4134–4142, <https://doi.org/https://doi.org/10.1002/2017GL072885>, 2017.



- Kottek, M., Grieser, J., Beck, C., Rudolf, B., and Rubel, F.: World Map of the Köppen-Geiger Climate Classification Updated, *Meteorologische Zeitschrift*, 15, 259–263, <https://doi.org/10.1127/0941-2948/2006/0130>, 2006.
- 485 Kottek, M., Grieser, J., Beck, C., Rudolf, B., and Rubel, F.: World Map of the Köppen-Geiger climate classification updated, <https://koeppen-geiger.vu-wien.ac.at/present.htm>, accessed: 2025-02-28, 2017.
- Lade, S., Steffen, W., Vries, W., Carpenter, S., Donges, J., Gerten, D., Hoff, H., Newbold, T., Richardson, K., and Rockström, J.: Human impacts on planetary boundaries amplified by Earth system interactions, *Nature Sustainability*, 3, 1–10, <https://doi.org/10.1038/s41893-019-0454-4>, 2020.
- Lade, S. J., Fetzer, I., Cornell, S. E., and Crona, B.: Prototype Earth system impact metric: code and data, 490 <https://doi.org/10.5281/zenodo.4738009>, accessed: 2025-02-28, 2021a.
- Lade, S. J., Fetzer, I., Cornell, S. E., and Crona, B.: A prototype Earth system impact metric that accounts for cross-scale interactions, *Environmental Research Letters*, 16, 115 005, <https://doi.org/10.1088/1748-9326/ac2db1>, 2021b.
- Luo, Y., Gerten, D., le Maire, G., Parton, W., Weng, E., Zhou, X., Keough, C., Beier, C., Ciais, P., Cramer, W., Dukes, J., Emmett, B., Hanson, P., Knapp, A., Linder, S., Nepstad, D., and Rustad, L.: Modeled Interactive Effects of Precipitation, temperature, and [CO₂] on Ecosystem 495 Carbon and Water Dynamics in Different Climatic Zones, *Global Change Biology*, 14, 1986–1999, <https://doi.org/10.1111/j.1365-2486.2008.01629.x>, 2008.
- Mohamed, A., DeClerck, F., Verburg, P. H., Obura, D., Abrams, J. F., Zafra-Calvo, N., Rocha, J., Estrada-Carmona, N., Fremier, A., Jones, S. K., Meier, I. C., and Stewart-Koster, B.: Securing Nature’s Contributions to People requires at least 20
- Ostberg, S., Lucht, W., Schaphoff, S., and Gerten, D.: Critical impacts of global warming on land ecosystems, *Earth System Dynamics*, 4, 500 347–357, <https://doi.org/10.5194/esd-4-347-2013>, 2013.
- Page, J., Abramowitz, G., De Kauwe, M., and Pitman, A.: Are Plant Functional Types Fit for Purpose?, *Geophysical Research Letters*, 51, <https://doi.org/10.1029/2023GL104962>, 2023.
- Piao, S., Friedlingstein, P., Ciais, P., de Noblet-Ducoudré, N., Labat, D., and Zaehle, S.: Changes in climate and land use have a larger direct impact than rising CO₂ on global river runoff trends, *Proceedings of the National Academy of Sciences*, 104, 15 242–15 247, 505 <https://doi.org/10.1073/pnas.0707213104>, 2007.
- Richardson, K., Steffen, W., Lucht, W., Bendtsen, J., Cornell, S. E., Donges, J. F., Drüke, M., Fetzer, I., Bala, G., von Bloh, W., Feulner, G., Fiedler, S., Gerten, D., Gleeson, T., Hofmann, M., Huiskamp, W., Kummu, M., Mohan, C., Nogués-Bravo, D., Petri, S., Porkka, M., Rahmstorf, S., Schaphoff, S., Thonicke, K., Tobian, A., Virkki, V., Wang-Erlandsson, L., Weber, L., and Rockström, J.: Earth beyond six of nine planetary boundaries, *Science Advances*, 9, eadh2458, <https://doi.org/10.1126/sciadv.adh2458>, 2023.
- 510 Runge, J., Bathiany, S., Bollt, E., Camps-Valls, G., Coumou, D., Deyle, E., Glymour, D., Kretschmer, M., Mahecha, M., Muñoz-Marí, J., van Nes, E., Peters, J., Quax, R., Reichstein, M., Scheffer, M., Schölkopf, B., Spirtes, P., Sugihara, G., Su, J., Zhang, K., and Zscheischler, J.: Inferring causation from time series in Earth system sciences, *Nature communications*, 10, <https://par.nsf.gov/biblio/10098201>, 2019.
- Schaphoff, S., von Bloh, W., Rammig, A., Thonicke, K., Biemans, H., Forkel, M., Gerten, D., Heinke, J., Jägermeyr, J., Knauer, J., Langerwisch, F., Lucht, W., Müller, C., Rolinski, S., and Waha, K.: LPJmL4 – a dynamic global vegetation model with managed land – 515 Part 1: Model description, *Geoscientific Model Development*, 11, 1343–1375, <https://doi.org/10.5194/gmd-11-1343-2018>, 2018.
- Sterling, S., Ducharne, A., and Polcher, J.: The impact of global land-cover change on the terrestrial water cycle, *Nature Climate Change*, 3, 13 688–, <https://doi.org/10.1038/nclimate1690>, 2013.
- Tobian, A., Gerten, D., Fetzer, I., Schaphoff, S., Andersen, L., Cornell, S., and Rockström, J.: Climate change critically affects the status of the land-system change planetary boundary, *Environmental Research Letters*, 19, <https://doi.org/10.1088/1748-9326/ad40c2>, 2024.



- 520 Todeschini, R., Ballabio, D., Termopoli, V., and Consonni, V.: Extended multivariate comparison of 68 cluster validity indices. A review, *Chemometrics and Intelligent Laboratory Systems*, 251, 105–117, <https://doi.org/10.1016/j.chemolab.2024.105117>, 2024.
- Udvardy, M.: *A Classification of the Biogeographical Provinces of the World*, International Union for Conservation of Nature and Natural Resources, 1975.
- Zhou, S., Yu, B., Lintner, B., Findell, K., and Zhang, Y.: Projected increase in global runoff dominated by land surface changes, *Nature*
- 525 *Climate Change*, 13, 1–8, <https://doi.org/10.1038/s41558-023-01659-8>, 2023.